Reviews in Mineralogy & Geochemistry
Vol. 62, pp. 193-230, 2006

Thermodynamics of Water Solubility and Partitioning

Hans Keppler
Bayerisches Geoinstitut
Universität Bayreuth
95440 Bayreuth, Germany
e-mail: Hans.Keppler@uni-bayreuth.de

Nathalie Bolfan-Casanova
Laboratoire Magmas et Volcans - CNRS UMR 6524
63038 Clermont-Ferrand cedex, France
e-mail: N.Bolfan@opgc.univ-bpclermont.fr

INTRODUCTION

When it was realized that nominally anhydrous minerals could be a major storage site of water in the mantle (Smyth 1987; Bell and Rossman 1992), it also became rather obvious that many mantle samples probably have lost most of their water during ascent (e.g., Ingrin and Skogby 2000). While analyses of natural samples therefore in many circumstances only provide a lower limit of the actual water content in the mantle, measurements of water solubility give an upper limit of the amount of water that might be stored in a mineral. Experimental measurements of water solubility have therefore naturally evolved in the last decades as a major tool for understanding the water storage capacity of the mantle.

Closely related to studies of water solubility are studies of water partitioning among minerals. If the water solubility in two minerals is known under given conditions, the partition coefficient is just the ratio of the water solubilities under the same conditions, provided that the composition of the fluid coexisting with the two minerals is the same. Since the pioneering work of Bai and Kohlstedt (1992) and of Kohlstedt et al. (1996), the water solubility in all major upper mantle minerals has been studied as well as the partitioning of water between the minerals of the lower mantle and the transition zone.

Solubility studies by themselves do not directly give the water content in the mantle. They constrain the storage capacity of the mantle, i.e., the maximum amount of water that may be stored, if the mantle were water-saturated. However, as most of the mantle is very likely water-undersaturated, the actual water content is probably far below the storage capacity.

Estimates of the actual abundance and distribution of water in the mantle may be obtained by combining solubility and partitioning data with direct observations of water contents in the upper mantle. If one assumes chemical equilibrium throughout the mantle one can model the water abundance in the transition zone and the lower mantle using experimentally derived water partition coefficients. This was first demonstrated by Bolfan-Casanova et al. (2000) and there is evidence from direct geophysical observations that this model is not too far away from reality (Huang et al. 2005; see also Hirschmann 2006). Whether the water distribution in the Earth's interior really approaches chemical equilibrium is, however, uncertain, although the relatively high diffusion coefficients of hydrogen in minerals (Ingrin and Blanchard 2006; this volume) and the high mobility of aqueous fluids would favor an equilibrium distribution. Ultimately, the actual abundance of water in the mantle can only be established by direct analyses of undegassed mantle samples and by geophysical observations.

1529-6466/06/0062-0009$05.00 DOI: 10.2138/rmg.2006.62.9

Finally, measurements of water solubility can help to constrain the recycling of water into the mantle in subduction zone, because they determine how much water can be retained in nominally anhydrous minerals when hydrous phases break down and release an aqueous fluid.

BASIC THERMODYNAMICS OF WATER SOLUBILITY AND PARTITIONING

The meaning of the term "water solubility"

At relatively low pressures, water solubility in a mineral can be conveniently defined as the equilibrium water content of the respective mineral coexisting with an aqueous fluid.

This definition is often meant to imply that the water activity in the fluid is close to unity. However, at high pressures and temperatures, the solubility of silicates in aqueous fluids becomes appreciable. In this situation, water activity in the fluid can be greatly reduced (e.g., Mibe et al. 2002). Naturally, the reduction of water activity will also lead to reduced equilibrium water contents in the coexisting minerals. This can be a problem if a thermodynamic model of water solubility in a mineral is calibrated at low P and T, where water activity in the fluid is close to unity and if this model is then extrapolated to much higher pressures and temperatures. In this case, the equilibrium water contents in minerals will be significantly overestimated, because the model predicts water solubilities in equilibrium with a hypothetical fluid consisting of essentially pure water, while in reality, water activity in the fluid may be significantly depressed due to dissolved silicate components.

Probably in all silicate-water systems, silicate melt and aqueous fluid become completely miscible at very high pressures and temperatures (Shen and Keppler 1997; Bureau and Keppler 1999; Kessel et al. 2005). The critical curve, which defines the pressure and temperature conditions where the solvus between fluid and melt closes, has been mapped out for some compositions. Some terms that are meaningful below the critical curve cannot be applied anymore at the "supercritical" pressures and temperatures beyond the critical curve. For example, one cannot define a water-saturated melt anymore, because this would imply a silicate melt coexisting with a separate aqueous fluid phase, which is impossible under conditions where fluid and melt are completely miscible. For the same reason, one cannot define the water solubility in a mineral in a simple way anymore, if the mineral coexists with a silicate melt, because in most cases, the water content of the melt and therefore the water activity imposed by the melt will depend on the bulk composition of the system studied (e.g., they will depend on the amount of water loaded into a sample capsule).

There are some circumstances, however, where one can define the term "water solubility" in a thermodynamically meaningful way even at pressures and temperatures beyond the critical curve. This is possible if the phase assemblage is invariant at given P und T and therefore buffers water activity and water solubility in all coexisting phases. Demouchy et al. (2005) studied the water content in Mg_2SiO_4 wadsleyite coexisting with $MgSiO_3$ clinopyroxene and a hydrous silicate melt in the system MgO-SiO_2-H_2O. According to the phase rule, the coexistence of three phases in a three-component system leaves two degrees of freedom. If pressure and temperature are fixed, these two degrees of freedom are used up and the system is invariant, i.e., the composition and therefore the water content of all phases will be a function of pressure and temperature only. Increasing the bulk water content in the experimental charge at constant P and T will simply increase the melt fraction without changing melt composition. Under these circumstances, it is justified to call the measured water content of wasleyite the water solubility in wadsleyite in equilibrium with a hydrous melt and clinopyroxene. It should be noted, however, that this is a definition of water solubility which is very different from the one generally used at lower pressures.

In numerous experimental studies, water contents of run products were measured and very often, these water contents were called "water solubility" without reference to any proper definition of this term. In many cases the term "water solubility" was even used in experiments were the phases investigated neither coexisted with a hydrous fluid nor with a hydrous silicate melt. This should be strictly avoided. Throughout this article, we will use the term water solubility according to the following definitions:

> Definition 1: Water solubility is the equilibrium water content of a mineral coexisting with an aqueous fluid phase.
>
> Definition 2: Water solubility is the equilibrium water content of a mineral coexisting with a hydrous melt in a phase assemblage that buffers the compositions of all coexisting phases in such a way that the composition of each phase only depends on pressure and temperature.

Throughout the discussion of water solubility in upper mantle minerals, we will usually refer to definition 1. Definition 2 will only be used in a few cases at pressures and temperatures of the deepest upper mantle, the transition zone or the lower mantle, i.e., at conditions that are likely to be beyond the critical curve in the systems considered.

Thermodynamics of water solubility

"Water" or "hydrogen" is dissolved in nominally anhydrous minerals as OH groups or rarely as molecular water. Molecular hydrogen (H_2) is probably an important diffusing species in these minerals, particularly during dehydration processes that involve the oxidation of ferrous iron or during hydration processes involving reduction of ferric iron. However, it has never been demonstrated that molecular hydrogen would contribute significantly to the storage of hydrogen in these minerals, although this may be possible under very reducing conditions. One can therefore rather safely assume that under normal circumstances, all hydrogen in a nominally anhydrous mineral will be present as OH groups or as molecular water. Since the chemical composition of silicates is usually expressed in the form of oxides, the terms "hydrogen solubility" and "water solubility" essentially have the same meaning.

The thermodynamics of water solubility is primarily controlled by the type of OH defect that forms. These may be isolated OH groups, pairs of OH groups or the "hydrogarnet defect" which is a cluster of four OH groups (Table 1).

Isolated OH groups may form by the direct substitution of a proton for a univalent cation such as Na^+ or Li^+, by the substitution of a trivalent cation and a proton for a tetravalent cation (e.g., $Al^{3+} + H^+$ for Si^{4+}) or by the substitution of a trivalent cation and a proton for two divalent cations (e.g., $Al^{3+} + H^+$ for 2 Mg^{2+}). The latter two substitution mechanisms are very important for the dissolution of water in aluminous orthopyroxene (Rauch and Keppler 2002; Mierdel 2006). The reaction between water and the mineral can be written as

$$H_2O_{fluid} + O_{mineral} = 2\ OH_{mineral} \tag{1}$$

where O is some unprotonated oxygen atom in the structure of the mineral. The equilibrium constant K_1 of this reaction is

$$K_1 = \frac{a_{OH}^2}{f_{H_2O} a_O} \tag{2}$$

where f_{H_2O} is the water fugacity. If the concentration of OH, i.e., the "water solubility" is proportional to the activity of OH and if the activity of the unprotonated oxygen atoms is constant, which is very likely at the low OH concentrations usually involved, this equation implies that water solubility should be proportional to the square root of water fugacity:

$$c_{water} \sim f_{H_2O}^{0.5} \tag{3}$$

Table 1. Hydrogen-bearing defects in nominally anhydrous minerals.

Substitution mechanism	Mineral	Reference
	---------- *Isolated protons* ----------	
$H^+ + Al^{3+} \leftrightarrow 2\ Mg^{2+}$	orthopyroxene	Mierdel (2006)
$H^+ + Al^{3+} \leftrightarrow Si^{4+}$	orthopyroxene	Rauch and Keppler (2002)
$H^+ + B^{3+} \leftrightarrow Al^{3+}$	B-rich olivine	Sykes et al. (1994)
$H^+ + Li^+ \leftrightarrow Mg^{2+}$	possibly in pyrope	Lu and Keppler (1997)
	---------- *Proton pairs* ----------	
$2\ H^+ \leftrightarrow Mg^{2+}$	olivine	Smyth, pers. comm.
	enstatite	Rauch and Keppler (2002)
	wadsleyite	Smyth (1987)
	ringwoodite	Smyth et al. (2003)
	possibly $MgSiO_3$ perovskite	Ross et al. (2003)
$2\ H^+ + Mg^{2+} \leftrightarrow Si^{4+}$	possibly ringwoodite	Kudoh et al. (2000)
interstitial H_2O	feldspars	Johnson and Rossman (2004)
	--------- *Cluster of four protons* ----------	
$4\ H^+ \leftrightarrow Si^{4+}$	garnet	Ackermann et al. (1983) Lager et al. (2005)

OH-pairs, i.e., two OH groups that cannot dissociate away from each other, typically form when two protons substitute for divalent cations, such as Mg^{2+}. This is believed to be an important substitution mechanism in olivine and in Al-free enstatite. Alternatively, OH pairs may also be generated by the substitution of two protons and a divalent cation for a tetravalent cation. Such a substitution would for example be the replacement of Si^{4+} by Mg^{2+} plus two protons, although such a substitution mechanism appears to be hardly considered in most studies. Reactions leading to OH pairs may be written as

$$H_2O + O = (OH)_2 \tag{4}$$

where $(OH)_2$ is the pair of OH groups. The equilibrium constant K_2 of this reaction is

$$K_2 = \frac{a_{(OH)_2}}{f_{H_2O} a_O} \tag{5}$$

Assuming that the concentration of OH is proportional to the activity of OH, this equation implies that water solubility should be directly proportional to the water fugacity:

$$c_{water} \sim f_{H_2O} \tag{6}$$

The same kind of relationship would be obtained if water were dissolved as molecular H_2O.

Finally, four protons may substitute for a tetravalent cation, such as Si^{4+} in the hydrogarnet defect $(OH)_4$. This may be written as

$$2\ H_2O + 2\ O = (OH)_4 \tag{7}$$

The equilibrium constant K_3 of this reaction is

$$K_3 = \frac{a_{(OH)_4}}{f_{H_2O}^2 a_O^2} \tag{8}$$

This equation implies that water solubility should be proportional to the square of water fugacity:

$$c_{water} \sim f_{H_2O}^2 \tag{9}$$

Different substitution types—isolated OH groups, OH pairs and the hydrogarnet defect—can therefore be distinguished by differences in the dependence of water solubility on water fugacity.

Equilibrium constants are related to the Gibbs free energy ΔG of the respective reaction by:

$$-RT\ln K = \Delta G = \Delta H^{1bar} - T\Delta S^{1bar} + \Delta V^{solid}\,(P\text{-}1\text{ bar}) \tag{10}$$

In this equation, the effect of pressure on the thermodynamic properties of the fluid is contained in the water fugacity. ΔH^{1bar} is the reaction enthalpy at 1 bar, ΔS^{1bar} is the reaction entropy at 1 bar and ΔV^{solid} is the volume change of the solids. R is the gas constant, T is temperature and P is pressure. By inserting the expressions for the equilibrium constants (Eqns. 2, 5, or 8) in this equation and by assuming that (1) the activity of the dissolved OH species is proportional to the concentration of dissolved water and that (2) the activity of the unprotonated oxygen atoms remains essentially constant, one obtains:

$$c_{water} = A f_{H_2O}^n \exp\left(-\frac{\Delta H^{1bar} + \Delta V^{solid} P}{RT}\right) \tag{11}$$

where A is a constant which essentially contains the entropy of reaction and n is an exponent related to the dissolution mechanism of OH: $n = 0.5$ for isolated OH groups, $n = 1$ for OH pairs (or molecular water), $n = 2$ for the hydrogarnet defect. Experimentally derived parameters for Equation (11) applied to the water solubility in a variety of nominally anhydrous minerals are compiled in Table 2.

The significance of the term ΔV^{solid} in Equation (11) requires some further discussion. The reactions leading to the dissolution of water in minerals were described in a somewhat

Table 2. Thermodynamic models for water solubility in minerals.

Mineral	A (ppm/bar^n)	n	ΔV^{solid} (cm^3/mol)	ΔH^{1bar} (kJ/mol)	Reference
Olivine	0.0066	1	10.6	—	Kohlstedt et al. (1996)
	0.0147 *	1	10.2	—	Mosenfelder et al. (2006)
	0.54	1	10.0	50	Zhao et al. (2004)**
$MgSiO_3$ enstatite	0.0135	1	12.1	−4.56	Mierdel and Keppler (2004)
Aluminous enstatite[#]	0.042	0.5	11.3	−79.7	Mierdel (2006)
Jadeite	7.144	0.5	8.02	—	Bromiley and Keppler (2004)
Cr-diopside[§]	2.15	0.5	7.43	—	Bromiley et al. (2004)
Pyrope	0.679	0.5	5.71	—	Lu and Keppler (1997)
Ferropericlase	0.0004	0.5	4.0	—	Bolfan-Casanova et al. (2002)

Tabulated parameters refer to Equation (11). Where no value for ΔH^{1bar} is given, the enthalpy term is missing because the temperature dependence of water solubility was not calibrated and the equations are strictly valid only at the temperatures they were calibrated.

Notes: * Recalculated from a value of $A = 2.45$ H/10^6 Si/MPa which in the original publication is probably misprinted as $A = 2.45$ H/10^6 Si/GPa; ** The equation by Zhao et al. (2004) also includes a term $\exp(\alpha x_{Fa}/RT)$, where a is 97 kJ/mol and x_{Fa} is the molar fraction of fayalite.; [#] This equation gives the water solubility coupled to Al of an Al-saturated enstatite. In order to get the total water solubility in Al-saturated enstatite, the water solubility in pure $MgSiO_3$ according to Mierdel and Keppler (2004) has to be added. [§] These data may reflect metastable equilibria.

simplified way by the Equations (1), (4), and (7). In reality, however, one has to consider that the conversion of an unprotonated oxygen atom to an OH group in the structure requires charge balancing by cation vacancies. Alternatively, this may also be described as a direct substitution of protons for cations. In pure enstatite, for example (Rauch and Keppler 2002) the main substitution mechanism is probably the direct replacement of Mg^{2+} by two protons. This may be written as

$$H_2O + MgSiO_3 = H_2SiO_3 + MgO \quad (12)$$

where H_2SiO_3 is the hydrous component in enstatite. The volume change of the solids during reaction is then

$$\Delta V^{solid} = V_{H_2SiO_3} + V_{MgO} - V_{MgSiO_3} \quad (13)$$

The physical meaning of ΔV^{solid} then depends on the behavior of the MgO formed during the reaction. If the MgO remains in solid solution in the pyroxene lattice during the reaction, then ΔV^{solid} is simply the volume change of the pyroxene structure upon hydration. However, if the MgO diffuses out of the crystal, ΔV^{solid} is the sum of the molar volume of MgO and the volume change of enstatite upon water dissolution. Interestingly, ΔV^{solid} for enstatite and also for olivine (Table 2) is quite close to the molar volume of MgO (11.25 cm^3/mol) and high-precision measurements of lattice constants of hydrous olivine (JR Smyth, pers. comm.) suggest that the incorporation of water causes a change of the unit cell volume comparable to ΔV^{solid} derived from fitting solubility data to Equation (11). This may perhaps imply that the MgO produced by reaction does indeed remain dissolved in the crystal structure and that the volume change of the lattice is largely due to the dissolution of this component.

It should be obvious from reactions such as the one shown in Equation (12), that water solubility will be sensitive to the activities of the oxide components involved. A substitution of protons for Mg^{2+} will proceed more easily at low MgO activity, while a substitution of protons for Si^{4+} will be favored by low silica activity. Eventually, it may even be possible to change the dissolution mechanism of water by changing the activities of MgO and SiO_2 and there is evidence that this may be possible for olivine at relatively low pressures (Lemaire et al. 2004). However, the most important chemical parameter influencing water solubility, is probably the activity of components that allow for coupled heterovalent substitutions, such as $Al^{3+} + H^+$ for Si^{4+} or $Al^{3+} + H^+$ for 2 Mg^{2+}. On the other hand, varying activities of different cations of the same valence, such as Mg^{2+} and Fe^{2+} should have a much smaller effect on water solubilities, if any.

Although Equation (11), which describes water solubility in minerals may look simple, the actual dependence of water solubility on pressure and temperature can be surprisingly complex. The water fugacity term in Equation (11) suggests that water solubility should increase with increasing water pressure. However, the term ΔV^{solid}, which is always positive, acts in the opposite direction. As a result, water solubility at a given temperature often first increases with pressure, reaches a maximum and then decreases at higher pressure. A physical explanation for this is that fluids are more compressible than solids and beyond a certain pressure the molar volume of water in the fluid may be smaller than the partial molar volume in the solid (e.g., Withers et al. 1998). A further increase in pressure then reduces water solubility. Similarly, the terms ΔH^{1bar} and $\Delta V^{solid}P$, which determine the temperature dependence at given pressure, may have opposite sign. At 1 bar, water solubility may decrease with temperature, while it increases with temperature at higher pressures.

Relationship between water solubility and partitioning

If two minerals α and β are in equilibrium with an aqueous fluid of the same composition, the solubility of water in each mineral is given by Equation (11) with the parameters relevant

for the respective mineral. The partition coefficient of water is then simply the ratio of the water solubilities in the two minerals:

$$c^{\alpha}_{water} = A_{\alpha}\, f^{n_{\alpha}}_{H_2O} \exp\left(-\frac{\Delta H^{1bar}_{\alpha} + \Delta V^{solid}_{\alpha} P}{RT}\right) \quad (14)$$

$$c^{\beta}_{water} = A_{\beta}\, f^{n_{\beta}}_{H_2O} \exp\left(-\frac{\Delta H^{1bar}_{\beta} + \Delta V^{solid}_{\beta} P}{RT}\right) \quad (15)$$

$$D^{\alpha/\beta}_{water} = \frac{c^{\alpha}_{water}}{c^{\beta}_{water}} = \frac{A_{\alpha}}{A_{\beta}}\, f^{n_{\alpha}-n_{\beta}}_{H_2O} \exp\left(-\frac{(\Delta H^{1bar}_{\alpha} - \Delta H^{1bar}_{\beta}) + (\Delta V^{solid}_{\alpha} - \Delta V^{solid}_{\beta})P}{RT}\right) \quad (16)$$

However, it is very important to note that at given P and T, the partition coefficient of water will only be independent of water activity, if the exponent n is the same for both minerals, i.e., if water is dissolved in both minerals as isolated OH groups or as OH pairs or as the hydrogarnet defect. If, however, the dissolution mechanism of water in the two minerals is different, the partition coefficient will depend on water activity. For example, if in mineral α water is dissolved as OH pairs, while in mineral β water is dissolved as isolated OH groups, $D^{\alpha/\beta}_{water}$ will increase with the square root of water activity at constant pressure and temperature. A similar effect of water activity on partition coefficients may occur for mineral/melt partitioning.

EXPERIMENTAL STRATEGIES FOR MEASURING WATER SOLUBILITY AND WATER PARTITION COEFFICIENTS

Annealing experiments

Annealing experiments are probably the most simple procedure for measuring water solubility in a mineral. In a typical annealing experiment, a preexisting crystal (natural or synthetic) is exposed to an aqueous fluid under controlled conditions of pressure, temperature and possibly oxygen fugacity. After a run duration which is deemed sufficient to reach equilibrium the charge is quenched and the water content of the crystal is measured. Most of the early studies on water solubility in minerals were carried out in this way (e.g., Bai and Kohlstedt 1992, 1993; Kohlstedt et al. 1996; Lu and Keppler 1997).

The main advantage of annealing experiments is the fact that one can easily obtain large and oriented single crystals. There are potential problems due to intense cracking of the original single crystal during compression or decompression of the experimental charges in the piston cylinder press or multi-anvil apparatus, but these problems can be solved by using low-friction assemblies (e.g., Bromiley et al. 2004).

Reaching chemical equilibrium can be a major problem in annealing experiments. In most silicate minerals, the dissolution of water is probably coupled to cation vacancies. Unless the crystal already contains a high population of vacancies, which only need to be "decorated" by protons, this means that equilibrium water solubilities can only be achieved if cations are able to diffuse out of the crystal during the run. In particular for cations with very low diffusion coefficients such as Si^{4+}, this is nearly impossible for mm-sized crystals during reasonable run durations. Accordingly, annealing experiments do not necessarily reach equilibrium, even if no evidence for diffusion profiles is seen in the samples. However, if overgrowth rims form during annealing experiments, the water contents observed in these rims may represent true equilibrium solubility.

Mosenfelder et al. (2006) demonstrated that identical water contents and virtually identical infrared spectra are obtained for olivine of natural composition, no matter whether

single crystals were annealed in a hydrous fluid or whether crystals were grown under water-saturated conditions. On the other hand, the same authors noted that water concentrations obtained by hydrous annealing of pure forsterite single crystals are one order of magnitude lower than the water concentration in forsterite crystals grown under nearly identical conditions. This is probably due to the slower diffusion kinetics in forsterite, which contains less mobile defects than olivine.

During annealing of a chromian diopside, Bromiley et al. (2004) observed clear evidence for disequilibrium. In particular, short run durations first yielded anomalously high water contents, which later decreased during the course of the experiment (Fig. 1). Probably, the initial incorporation of water in these and many other experiments is due to the local reduction of Fe^{3+} and the incorporation of H^+ close to the Fe^{2+} produced by the reduction process. Upon longer annealing times, the defects can then migrate to a more stable environment. Whether a real stable equilibrium or only a metastable state is ultimately reached in these experiments probably depends on the available populations of cation vacancies and their diffusivities. In any case, the question of attainment of equilibrium needs to be carefully addressed in any study of water solubility in minerals by annealing experiments.

Even if annealing experiments do not reequilibrate all defects, they can be useful for special applications. Mantle xenoliths that have lost most of their water during ascent may still contain defects (e.g., metal vacancies) that were related to the dissolution of water. It may then be possible to decorate these defects with hydrogen by annealing the sample in water under conditions where the diffusivity of the metal vacancies is low. In this way, it may ultimately be possible to reconstruct the original water content of a mantle mineral, even if it has lost all water during ascent to the surface (Kohlstedt and Mackwell 1998).

Crystallization experiments

In crystallization experiments, crystals of the desired mineral are directly grown under water-saturated conditions. In these experiments, attainment of equilibrium should be much

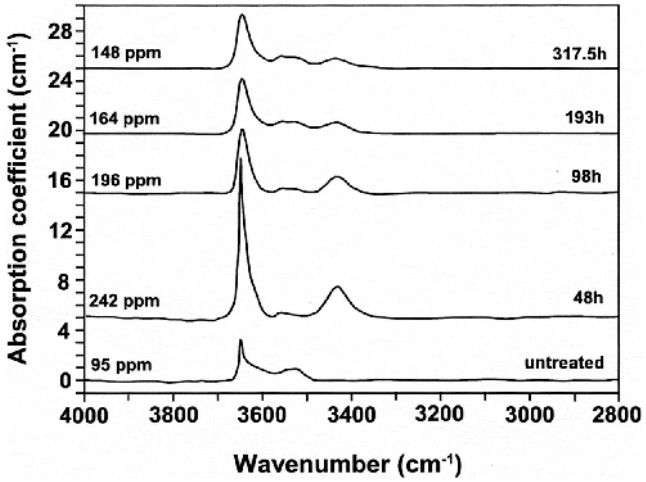

Figure 1. Infrared spectra of natural chromian diopside annealed in water at 15 kbar and 1100 °C under Ni-NiO buffer conditions for different run durations. Bulk water contents are given in ppm H_2O by weight. Initially, very high water contents are produced after short run durations, probably due to local reduction of Fe^{3+} to Fe^{2+}. Diffusion of defects towards a more stable environment leads to a reduction of water contents after longer run durations. From Bromiley et al. (2004).

less of a problem than with annealing experiments. However, often it is quite difficult to produce clear and inclusion-free crystals that are sufficiently large to be oriented for polarized FTIR measurements. One way to overcome this problem is to grow the crystals from a melt by slow cooling (e.g., Stalder 2002; Lemaire et al. 2004). However, the water content of such crystals will only represent true water solubility if it can be demonstrated that the melt was water-saturated, i.e., in equilibrium with a separate aqueous fluid phase throughout the entire experiment. Moreover, the method can only be applied to temperatures above the water-saturated solidus and if water solubility is a function of temperature, it is difficult to interpret the water solubility, as it is not precisely known to which temperature they correspond.

An alternative approach to generate large single crystals of silicates at constant temperature was introduced by Mierdel and Keppler (2004). In these experiments, alternating layers of starting mixtures with different compositions (e.g., with silica excess and deficient in silica) are introduced into the sample capsule, so that the phase of interest can only nucleate at the boundary between the layers. With this method, it was possible to grow mm-sized water-saturated crystals of enstatite at relatively low temperatures. However, because these experiments necessarily involve a gradient in activities (e.g., silica activity), it is not possible to buffer all activities during the growth of the crystal.

WATER IN UPPER MANTLE MINERALS

Water solubility in and the Al content of orthopyroxenes as "geohygrometer"

Although orthopyroxene is less abundant in the upper mantle than olivine, it is probably the most important host of water, particularly in the shallow part of the upper mantle. Moreover, water solubility in orthopyroxene is particularly well understood and calibrated.

Water solubility in pure $MgSiO_3$ enstatite was measured by Rauch (2000), Rauch and Keppler (2002) and Mierdel and Keppler (2004). At 1100 °C, water solubility increases with pressure to a maximum of 867 ppm by weight at 75 kbar and then decreases at higher pressures to 714 ppm at 100 kbar in the stability field of high-clinoenstatite. While water solubility at room pressure decreases with temperature, it significantly increases with temperature at pressures above about 10 kbar (Fig. 2). The entire available data set can be described by one single equation of the type of Equation (11) with the fit parameters given in Table 2. Stalder and Skogby (2002) report a water content in an Al-free enstatite crystallized from a water-saturated melt at 25 kbar and 1400-1150 °C of 29.5 ppm H which corresponds to 280 ppm of water, in reasonable agreement with Figure 2. At much higher pressures, Inoue et al. (1995) and Yamada et al. (2004) report water contents between 0.3 and 0.8 wt% in high-clinoenstatite coexisting with a hydrous melt between 1200 and 1500 °C and 130-155 kbar. Since these water contents were measured by SIMS, it is not certain whether they are representative for the chemically dissolved water in the sample or whether some of the water may come from hydrous inclusions.

The infrared spectra of synthetic hydrous enstatite crystals are simple (Fig. 3). They consist of a strong narrow band at 3363 cm^{-1} and a weak broader band at 3064 cm^{-1}, which are both strongly polarized parallel *c*. In samples synthesized below 1000 °C, the strong band may be split into two components, possibly reflecting a very subtle change in the pyroxene structure. In addition, there are some very weak features at higher frequencies. All observations are consistent with a direct substitution of Mg^{2+} by two protons. Silica activity (buffering by excess SiO_2 or by forsterite) appears to have very little influence both on water solubility and on the type of infrared spectra observed.

Aluminum has a drastic effect on water solubility in enstatite (Rauch 2000; Rauch and Keppler 2002; Stalder and Skogby 2002; Mierdel 2006; Mierdel et al. in prep.). The water solubility in enstatite saturated with aluminum (i.e., in equilibrium with $MgAl_2O_4$ spinel or

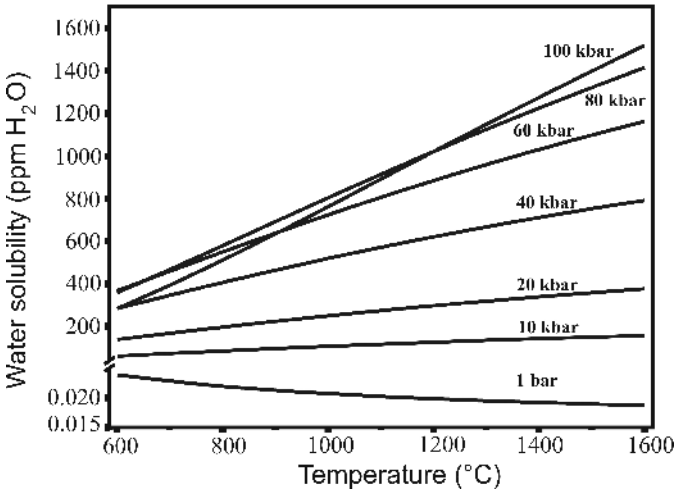

Figure 2. Water solubility in pure $MgSiO_3$ enstatite according to the thermodynamic model of Mierdel and Keppler (2004).

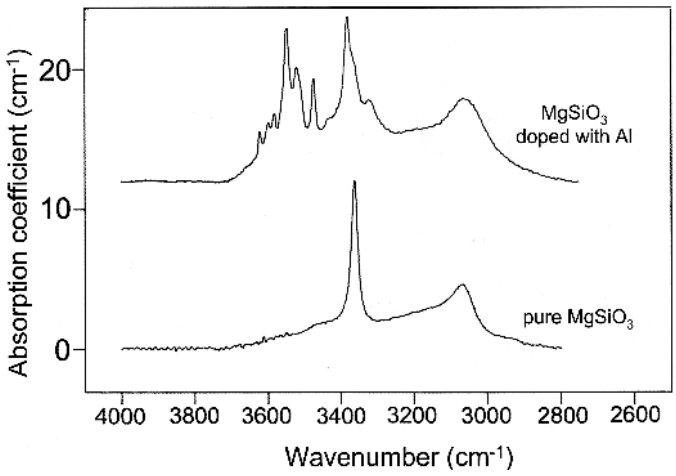

Figure 3. Infrared spectra of water-saturated pure $MgSiO_3$ enstatite and of Al-doped enstatite, synthesized at 15 kbar and 1100 °C. After Rauch and Keppler (2002).

with pyrope) may be more than hundred times higher than the water solubility in Al-free enstatite under the same conditions (Mierdel 2006). In the presence of aluminum, new bands appear in the infrared spectrum of hydrous enstatite (Fig. 3), in addition to the bands seen in Al-free enstatite. At very high aluminum contents, the bands tend to broaden and to overlap, so that most of the fine structure is lost.

In the Earth's mantle, orthopyroxene (enstatite) coexists with olivine, clinopyroxene and an aluminum-rich phase ($MgAl_2O_4$-rich spinel in the spinel peridotite stability field and pyrope-rich garnet in the garnet peridotite field). Mierdel (2006) and Mierdel et al. (in prep.) calibrated the water solubility in enstatite coexisting with olivine and $MgAl_2O_4$ spinel or pyrope as a function of pressure and temperature. Water solubility in Al-saturated enstatite

reaches values close to 1 wt% at 15 kbar and 800 °C. Water solubility decreases rapidly both with increasing pressure and temperature. A thermodynamic model calibrated by Mierdel (2006) and Mierdel et al. (in prep) describes water solubility in aluminum-saturated enstatite as the sum of two terms, one term being equal to the water solubility in Al-free enstatite and one term describing the water solubility related to the incorporation of aluminum. Both terms are described by equations of the type of Equation (11), with the respective fit parameters given in Table 2. A notable difference between the two equations used is in the exponent of the water fugacity. While the term for the water solubility in the absence of Al has an exponent of 1, implying incorporation of OH pairs charge balanced by a magnesium vacancy, the term describing the water solubility related to aluminum has an exponent of ½, implying the dissolution of water as isolated OH groups. Water solubilities in Al-saturated enstatite predicted by the thermodynamic model are shown in Figure 4.

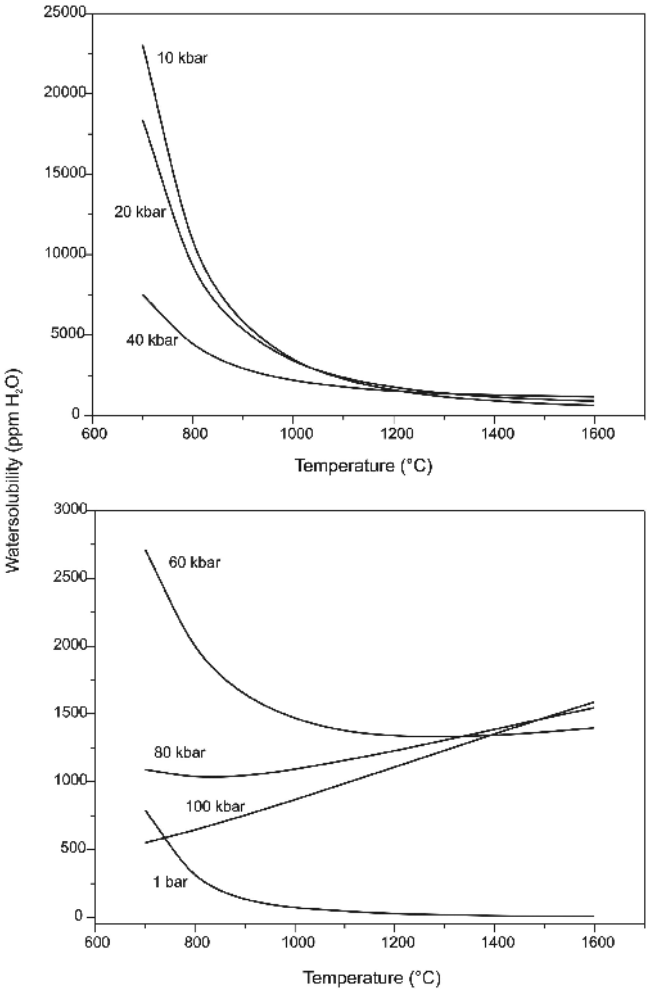

Figure 4. Water solubility in Al-saturated enstatite as a function of pressure and temperature. The term "Al-saturated" refers to enstatite in equilibrium with forsterite and the stable aluminous phase, i.e., $MgAl_2O_4$ spinel or pyrope, depending on pressure. After the thermodynamic model by Mierdel (2006) and Mierdel et al. (in prep.).

Rauch (2000) and Rauch and Keppler (2002) originally assumed that aluminous pyroxenes dissolve water primarily as $Mg_2(AlH)SiO_6$ component, i.e., by a coupled substitution of tetrahedral $Al^{3+} + H^+$ for Si^{4+}. This would imply that the ratio of tetrahedral over octahedral Al in an orthopyroxene should increase with the water content, as in the absence of water, Al is dissolved as Tschermak component $MgAlAlSiO_6$ with a ratio of tetrahedral to octahedral Al of 1:1. The ratio of tetrahedral over octahedral Al in an orthopyroxene could therefore be a potential "geohygrometer," which may be a measure of the original water content of a pyroxene and therefore a measure of water fugacity in the mantle. Because of the much slower diffusion of Al as compared to water, this geohygrometer may still be applicable even if a mantle pyroxene has lost all of its water during ascent to the surface. However, Kohn et al. (2005) presented ^{27}Al NMR evidence suggesting that water has little effect on the intracrystalline partitioning of Al in enstatite and that even water-rich aluminous pyroxenes still contain tetrahedral and octahedral Al in an approximate 1:1 ratio. This is also consistent with results by Stalder and Skogby (2002) and Stalder (2004) who suggested that a large fraction of Al in hydrous orthopyroxene is dissolved as Tschermak component.

Mierdel (2006) carried out extensive electron microprobe and infrared analyses of aluminous enstatite crystals synthesized under water-saturated conditions at pressures between 15 and 35 kbar and at temperatures between 800 and 1100 °C. According to these data and single crystal structure refinements (Mierdel et al. in prep.; Smyth et al. in prep.), aluminum is incorporated in enstatite by three substitution mechanisms, corresponding to the following three end members:

Mg Al Al Si O_6	(Tschermak component)
Mg Mg (AlH) Si O_6	("Rauch" component; Rauch 2000)
H Al Si Si O_6	("Jadeite-like" component)

In most crystals analyzed, the Rauch component and the jadeite-like component appear to occur at a molar ratio of 1:1, implying an equal ratio of tetrahedral over octahedral aluminum, equivalent to a substitution by a "hydro-Tschermak-component" $H_2AlAlSiO_6$ This may perhaps be related to a minimization of distortions of the pyroxene structure, because the Rauch substitution would tend to increase the volume of the tetrahedral sites, while the jadeite-like substitution would reduce the volume of the octahedral sites. In two experiments, however, microprobe analyses suggest that virtually all Al is dissolved as Rauch component, as originally proposed by Rauch (2000) and Rauch and Keppler (2002). The reason for this is unclear.

Interestingly, the aluminum contents of water-saturated enstatite crystals coexisting with $MgAl_2O_4$ spinel or pyrope are significantly higher than predicted by previous experimental studies and models of aluminum solubility in enstatite (MacGregor 1974; Dankwerth and Newton 1978; Perkins et al. 1981; Gasparik 2003), particularly at low temperatures and pressures, where water solubility is high (Fig. 5). Although in many previous studies on aluminum solubility in enstatite, water was added to the charge, these experiments were probably not water-saturated, because in the absence of special precautions, water is easily lost from the sample capsules in piston cylinder experiments (Truckenbrodt and Johannes 1999; Freda et al. 2001). Moreover, most of these previous experiments were carried out at high temperatures, where water solubility in the aluminous enstatite is relatively low. The available thermodynamic models of aluminum solubility in enstatite therefore probably only describe the Tschermak-type solubility in the absence of water. Since both the Rauch component and the jadeite-like component imply a molar 1:1 ratio of aluminum to hydrogen, one would therefore expect that the "excess" of aluminum found in the hydrous pyroxenes (compare Fig. 5) correlates with the water solubility coupled to aluminum on a molar 1:1 ratio. This was observed by Mierdel (2006): within error, the molar fraction of water dissolved in the aluminous enstatite minus the water present in the Al-free enstatite under the same

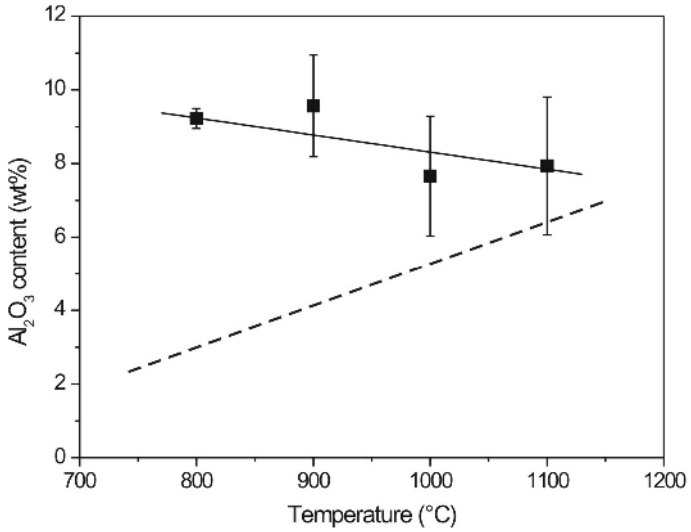

Figure 5. Aluminum content of enstatite in equilibrium with olivine, $MgAl_2O_4$ spinel and water at 15 kbar after Mierdel (2006). For comparison, the Al-solubility in orthopyroxene after Gasparik (2003) is shown (dashed line). The model of Gasparik probably only reflects aluminum solubility at low water activities, where the Tschermak-substitution dominates. In the presence of water, coupled substitutions of Al and H are possible at low temperatures which lead to elevated aluminum solubilities that were not included in existing thermodynamic models of aluminum in orthopyroxene. The "excess" aluminum content, i.e., the difference between the two curves in the figure at a given temperature correlates in a molar 1:1 ratio with the water content in the pyroxene due to aluminum. Above 1100 °C, the aluminum solubility in water-saturated orthopyroxene approaches the curve for anhydrous conditions.

conditions equals the molar fraction of excess aluminum found in these crystals, where excess aluminum means the difference between the measured aluminum content and that predicted by the model of Gasparik (2003). In this sense, Al in orthopyroxene is indeed a geohygrometer. In principle, it should be possible to determine the original water content of an orthopyroxene from the mantle simply by looking at its aluminum content. This can be done if the pressure and temperature conditions of the formation of this orthopyroxene are known. If the aluminum content in the pyroxene is higher than predicted based on calibrations of the Tschermak-type solubility, this suggests that the crystal originally contained water. The molar fraction of the water coupled to Al simply equals the molar fraction of excess Al observed. The observed water content can then be compared to the water content predicted by Equation (11) with the fit parameters in Table 2 as a function of P, T and water fugacity. If P and T are known with sufficient accuracy, the water fugacity in the mantle source of the pyroxene can be calculated.

Stalder (2004) and Stalder et al. (2005) showed that in addition to Al^{3+}, other trivalent ions, particular Fe^{3+} and Cr^{3+} also enhance water solubility in enstatite. However, in natural mantle orthopyroxenes Cr^{3+} and Fe^{3+} are much less abundant than Al^{3+}. Therefore, the effect of chromium and trivalent iron on water solubility in orthopyroxene is probably small. Similarly, some annealing experiments on natural orthopyroxenes reported by Rauch and Keppler (2002) suggest that limited substitution of Fe^{2+} for Mg^{2+} has little effect on water solubility. The main compositional control of water solubility in orthopyroxene certainly is aluminum activity, as first observed by Rauch (2000).

Water solubility in olivine

Olivine is compositionally simpler than orthopyroxene, with the Mg/Fe ratio being the

only important variable. This compositional simplicity contrasts with the diversity of infrared bands seen in natural olivines from mantle xenoliths and other sources (e.g., Miller et al. 1987; Matsyuk and Langer 2004).

The first experimental calibration of water solubility in olivine under mantle conditions was carried out by Kohlstedt et al. (1996). In this study, oriented single crystals of natural San Carlos olivine were annealed with excess water at 1100 °C and 25 to 130 kbar for run durations between 3 hours and more than 2 days. Oxygen fugacity was controlled by the Ni-NiO-buffer. At the beginning of the experiments, the olivine crystals were surrounded by a talc-brucite mixture, which reacted during the experiment to a mixture of forsterite and enstatite, i.e., silica activity in these experiments was buffered by the presence of enstatite. Water contents of run products were measured by FTIR using extinction coefficients after Paterson (1982). Water solubility was found to increase with pressure up to a maximum of 1510 ppm by weight at 12 GPa (Fig. 6; Table 2). The infrared spectra of the run product olivines were found to be dominated by strong bands at 3613 cm^{-1}, 3598 cm^{-1} and 3579 cm^{-1}.

Since the experiments by Kohlstedt et al. (1996) were carried out by annealing natural crystals, it may be questionable whether all defects were really reequilibrated in these experiments and whether the water contents measured really reflect equilibrium water solubilities (e.g., Matveev et al. 2001). This was tested by Mosenfelder et al. (2006). They carried out experiments with starting materials made of San Carlos olivine either as single crystals or as fine-grained powders. While in the first type of experiment, water diffuses into the crystals as in the study by Kohlstedt et al. (1996), in the second type of experiment large crystals grow at the expense of the fine-grained starting material and incorporate water during growth. Both types of experiments were found to yield similar water contents and similar infrared spectra at otherwise identical conditions (Fig. 7). The infrared spectra are also similar to those reported by Kohlstedt et al (1996). However, Mosenfelder et al. (2006) calculated water contents by applying a newly calibrated infrared extinction coefficient for water in

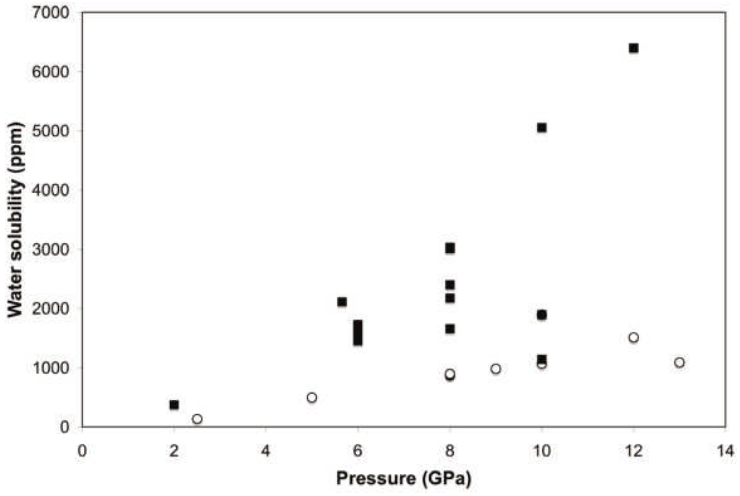

Figure 6. Water solubility in olivine. Shown are experimental results on San Carlos olivine by Kohlstedt et al. (1996; open circles) and by Mosenfelder et al. (2006; black squares). Both studies were mostly carried out at 1100 °C, but the data by Mosenfelder et al. (2006) include some experiments at 1000-1300 °C. Note that the difference between the two studies mostly results from the use of different infrared extinction coefficients for quantifying the water content of the run products. Fit parameters of the solubility laws resulting from the two studies are given in Table 2.

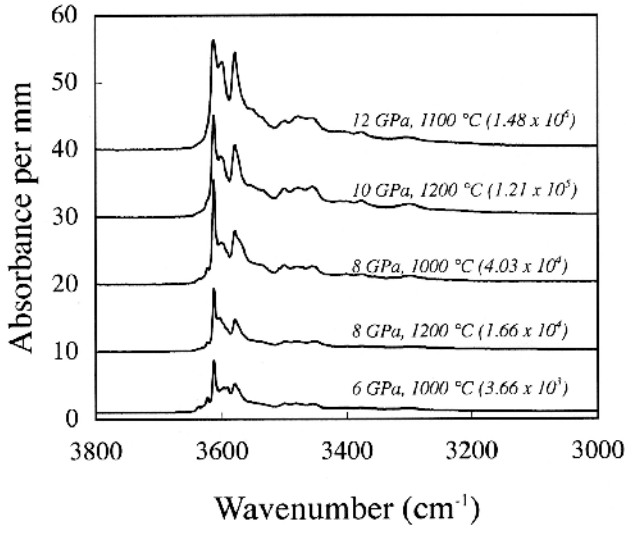

Figure 7. Infrared spectra (polarized parallel *a*) of water-saturated olivine from high-pressure experiments Numbers in brackets are water fugacities in GPa. From Mosenfelder et al. (2006).

olivine (Bell et al. 2003). This extinction coefficient generally yields water contents by a factor of 2-4 higher than those derived from the calibration of Paterson (1982) and therefore, the water solubilities in olivine obtained by Mosenfelder et al. are higher than those by Kohlstedt et al (Fig. 6). However, these differences are mostly due to the different extinction coefficients used. In all other aspects, both studies agree quite well; for example, they yield nearly the same value for ΔV^{solid}, the volume change of the solids during the dissolution of water (Table 2). Moreover, Mosenfelder et al. (2006) were also able to show that the infrared spectra of olivines hydrated at high pressure are similar, dominated by high-frequency bands around 3600 cm^{-1}, irrespective of the composition of the starting material (Fig. 8). The infrared spectra of the experimental samples are quite similar to those of some natural olivines from garnet peridotites (Fig. 9). Smyth et al (J. Smyth, pers. comm.) recently studied water solubility in pure forsterite at 120 kbar and 1100 to 1600 °C. They also found that the infrared spectra of their samples were dominated by high-frequency bands around 3600 cm^{-1}, as in the studies by Kohlstedt et al. (1996) and Mosenfelder et al. (2006). The type of infrared spectrum observed by Smyth et al. appears to be nearly independent of silica activity; spectra of forsterite coexisting with melt and enstatite are similar to the spectra of forsterite coexisting with melt and clinohumite. According to single crystal structure refinements by Smyth et al (J. Smyth, pers. comm.) the dominant dissolution mechanism of water in olivine appears to be the replacement of Mg^{2+} by 2 H^+, as suggested by the direct observation of cation vacancies on the M1 and M2 sites of Mg. This is entirely consistent with the exponent of 1 in the water fugacity term of Equation (11) (Table 2) describing water solubility in olivine as found by Kohlstedt et al (1996) and Mosenfelder et al. (2006). Moreover, the fact that Smyth et al. observe infrared spectra in chemically pure hydrous forsterite that are similar to those observed by Kohlstedt et al. (1996) and Mosenfelder et al. (2006) demonstrates that the dominant mechanism for the dissolution of water in olivine cannot be related to minor chemical impurities.

Zhao et al. (2004) observed at relatively low pressures (3 kbar) that water solubility in olivine increases significantly with temperature and also with Fe/Mg ratio (Table 2). Smyth et al. (J Smyth, pers. comm.) also observed that water solubility in pure forsterite approximately doubles from 1100 °C to 1250 °C.

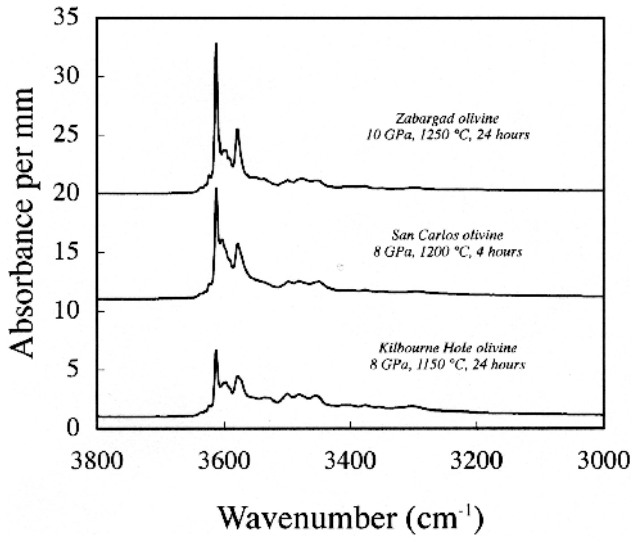

Figure 8. Infrared spectra (polarized parallel *a*) of water-saturated olivine grown from three different starting materials. Clearly, the main absorption bands seen in these samples are independent of the starting material. From Mosenfelder et al. (2006).

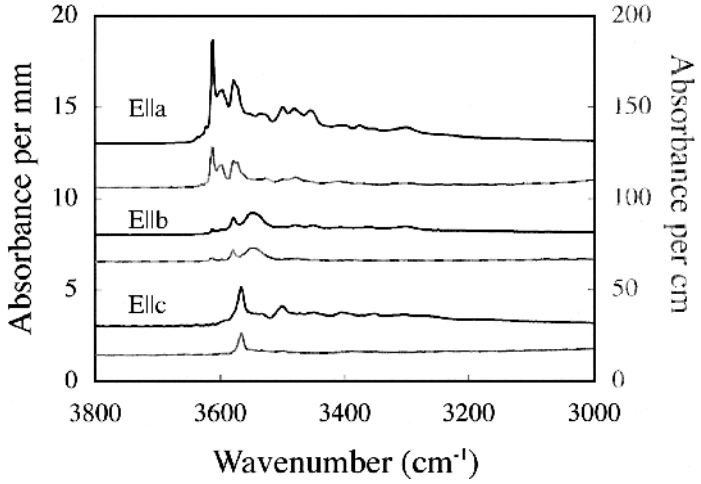

Figure 9. Polarized infrared spectra of a water-saturated olivine from an experiment at 8 GPa and 1150 °C (black) and from a natural crystal of olivine from a garnet peridotite (Bull peak diatreme, Arizona). The similarity of the spectra demonstrates that the experiments faithfully reproduce the defects found in natural olivines from the garnet peridotite field. From Mosenfelder et al. (2006).

Bai and Kohlstedt (1993) already noted that olivines may show infrared bands which behave differently in response to changes in the chemical environment. They distinguished "group I bands" above 3450 cm^{-1} from "group II bands" below 3450 cm^{-1}. The relative intensity of the group II bands was very much enhanced at oxidizing conditions, while they pretty much disappeared under reducing conditions.

Matveev et al. (2001) studied the water solubility in olivine buffered by orthopyroxene (high silica activity) or magnesiowüstite (low silica activity). The experiments were carried out at 1300 °C, Re-ReO_2 buffer conditions and mostly at 20 kbar. They observed that silica had a major effect on the infrared spectra observed in the run products. While the olivines in equilibrium with magnesiowüstite (low silica activity) showed infrared bands at high frequencies around 3600 cm^{-1} (group I of Bai and Kohlstedt), these bands disappeared in the runs buffered by orthopyroxene (high silica activity) while new bands appeared at low frequency in the range between 3400 and 3200 cm^{-1} (group II of Bai and Kohlstedt). Lemaire et al. (2004) observed a similar effect of silica activity on the infrared spectra of pure hydrous forsterite grown at 20 kbar and about 1500 °C. However, in their experiments, the bands at high frequency (group I) never disappeared completely.

From their study, Matveev et al. (2001) concluded:

(1) The ratio of group I over group II bands is an indicator of silica activity.

(2) Group I bands are due to tetrahedral Si vacancies, because they are enhanced at low silica activity.

(3) Group II bands are due to octahedral Mg vacancies, because they are enhanced at high silica / low MgO activity.

(4) Olivines from natural mantle xenoliths, which show the high-frequency group I bands are out of equilibrium with the surrounding mantle, because they appear to reflect a very low silica activity environment. This may reflect metasomatism by a very silica-poor medium, such as a carbonatite melt.

The work by Matveev et al (2001) has very much stimulated research into the significance of individual bands in the infrared spectrum of olivine. The dependence of the intensity ratio of group I over group II bands on silica activity is certainly real, at least at the low pressures (20 kbar) and high oxygen fugacities (Re-ReO_2-buffer) studied by Matveev et al. However, there are major problems with some of the interpretations by these authors:

(1) The assignment of group I and group II bands to silicon and magnesium vacancies does not explain why the intensity of the group II bands is greatly enhanced at high oxygen fugacity and why they tend to disappear at low oxygen fugacity (Bai and Kohlstedt 1993).

(2) The studies by Kohlstedt et al (1996), Mosenfelder (2006) and by Smyth et al. (J. Smyth, pers. comm.) all show that at high pressures above 20 kbar and under reasonable conditions of oxygen fugacity, hydrous olivines always exclusively show the high-frequency group I bands, independent of silica activity. Moreover, single crystal structure refinements suggest that these bands are primarily related to Mg^{2+} vacancies (J. Smyth, pers. comm.).

In order to reconcile all of the observations outlined above, we suggest the following model:

(1) Silicon vacancies are not important for dissolving water in olivine. This is consistent with experimental evidence that the hydrogarnet substitution in pyrope becomes unfavorable at high pressure, because of the large volume expansion of the tetrahedral site associated with this kind of defect (Withers et al. 1998).

(2) Throughout most of the mantel, in particular at high pressure and under reasonably reducing conditions, the main dissolution mechanism for water in olivine is the substitution of Mg^{2+} by proton pairs. This substitution mechanism is responsible for the prominent group I bands around 3600 cm^{-1}.

(3) Under conditions of high silica activity (which necessarily means low MgO activity)

and only at relatively low pressures, additional substitution mechanisms become important which lead to group II bands. At low MgO activity, the population of Mg vacancies will be particularly high. This charge deficiency on the Mg site may be compensated in the crystal by the oxidation of Fe^{2+} to Fe^{3+} and by simultaneous protonation. The group II bands may therefore be due to protonated vacancies close to an Fe^{3+} site. Therefore, it is not surprising that the intensity of group II bands, particularly those around 3300 cm^{-1} (Matveev et al. 2001; Bai and Kohlstedt 1993) increases both with oxygen fugacity and with silica activity. In the absence of iron or other trivalent ions, low MgO activity may lead to associated defects (clusters of Mg vacancies). The broad bands seen at about 3150-3200 cm^{-1} in pure hydrous forsterite (Lemaire et al. 2004) are probably related to such associated defects. This is consistent with the observation by Berry et al. (2005) that these bands disappear completely when titanium is added to the system. If Ti^{4+} enters the octahedral site of olivine, it can charge compensate not only the Mg^{2+} vacancy which it occupies, but also a neighboring vacancy. Therefore, no hydrogen can be stored in such vacancy pairs anymore once a suitable tetravalent cation is introduced into the system.

When comparing infrared spectra of olivines from high-pressure experiments and natural samples, the following things should be kept in mind:

(1) Most natural olivines have probably lost a large fraction of their initial water content during ascent (Ingrin and Skogby 2000). Probably, not all species of water will diffuse out of the crystal with the same rate. Water coupled to some cations with low diffusivity (such as Ti^{4+}) as well as water in planar defects may be particularly immobile. This may explain the prominence and great diversity of bands related to such species in the spectra of natural samples. For example, Berry et al. (2005) showed that the 3572 cm^{-1} band as well as the 3525 cm^{-1} band seen in many natural olivines are probably related to a Ti^{4+}-bearing defect cluster. However, the low abundance of Ti^{4+} in natural olivine makes it unlikely that this defect would contribute significantly to the bulk solubility of water in olivine at high water fugacities.

(2) Water loss during ascent of a xenolith is usually accompanied by oxidation, i.e., "water" is not lost as H_2O, but as H_2, produced by the simultaneous oxidation of Fe^{2+} to Fe^{3+}(Ingrin and Skogby 2000). As the intensity ratio of group I to group II bands is sensitive to oxidation state as well as to silica activity, one should be cautious in interpreting this intensity ratio as observed in natural samples in terms of silica activity alone (Matveev et al. 2005). Moreover, as olivines synthesized at high pressures only show group I bands even in equilibrium with enstatite, the predominance of these bands in natural samples does not imply that these samples are out of equilibrium with orthopyroxene.

(3) Experiments carried out under quite oxidizing conditions, such as the Re-ReO_2 buffer may generate enhanced intensities of group II bands that are not realistic for any natural sample.

(4) Differences in band positions by a few cm^{-1} relate to extremely subtle changes in chemical environment (essentially oxygen-oxygen distances), which should not be interpreted in terms of radically different substitution mechanisms.

From the discussion above, it is obvious that many details of the dissolution mechanism of water in olivine still need further investigation. The most serious problem, however, is related to the very different water solubilities in olivine obtained by applying either the Paterson (1982) or the Bell et al. (2003) calibrations of infrared extinction coefficients to the same samples. This difference has serious geological consequences as will be pointed out below. Further independent calibrations of infrared extinction coefficients and water contents in olivine would therefore be highly desirable.

Water solubility in garnet

Garnets have attracted a lot of attention as potential host of water because of the natural occurrence of katoite or "hydrogarnet" $Ca_3Al_2(H_4O_4)_3$. Katoite is a mineral with garnet structure, which can be considered as a grossular $Ca_3Al_2(SiO_4)_3$ with each of the Si^{4+} cations replaced by four protons. The structure of katoite is well studied. The four protons are located outside of the tetrahedral site, above the edges of the tetrahedron (Lager et al. 2005 and references therein). The infrared spectrum of hydrogarnet shows essentially one broad band at about 3600 cm^{-1} with a shoulder at 3660 cm^{-1} (Rossman and Aines 1991).

The first experimental evidence that the hydrogarnet defect may occur in pyrope-rich garnets relevant to the upper mantle was provided by Ackermann et al. (1983). They observed an absorption band close to 3600 cm^{-1} in the infrared spectrum of pyrope synthesized in the presence of excess water at 25 kbar and 1000 °C. A systematic study of water solubility in pyrope at 1000 °C and up to 130 kbar was carried out by Withers et al. (1998). They synthesized pyrope coexisting with excess SiO_2 from oxide mixes and observed the typical broad hydrogarnet band at 3600 cm^{-1} in the run products. Water solubility in garnet was found to increase with pressure up to about 1000 ppm at 40 kbar and then to decrease to nearly zero at pressures above 80 kbar. The decrease of water solubility at high pressures is probably due to the large volume expansion of the solids upon dissolution of water.

Lu and Keppler (1997) studied water solubility in pyrope-rich garnet at 1000 °C and up to 100 kbar by annealing a natural garnet sample from Dora Maira in water. Water solubility in this garnet was found to increase continuously to about 200 ppm at 100 kbar. The parameters obtained from a fit of the solubility data to an equation similar to Equation (11) suggest the dissolution of water as isolated OH groups in this sample (Table 2; note exponent ½ of water fugacity term). This is consistent with the infrared spectrum of the sample which is quite different from that observed by Withers et al (1998) for pure pyrope. In addition to a rather sharp band at 3600 cm^{-1}, there are three more bands around 3650 cm^{-1}. Possibly, the dissolution of water in this sample is coupled to chemical impurities.

Although there is still a need for more systematic studies of water solubility in garnets particularly as a function of bulk composition, the available data suggest that garnet is probably not an important host for water in the upper mantle, both because of its limited storage capacity for water and its low modal abundance.

Water solubility in clinopyroxene

Clinopyroxenes, particularly omphacites are among the most water-rich samples from mantle xenoliths (Skogby 2006). Due to its low modal abundance, clinopyroxene probably does not contribute very much to the bulk water storage capacity of the upper mantle. However, omphacites are likely to be important carriers for transporting water down into the mantle in subducted slabs.

Bromiley and Keppler (2004) investigated water solubility in pure jadeite at 600 °C and pressures up to 100 kbar. Infrared spectra of the synthetic hydrous jadeites show two prominent sharp peaks at 3373 cm^{-1} and 3613 cm^{-1} together with several weaker features. Band positions and polarizations suggest a water dissolution mechanism involving vacancies on the *M*2 site, consistent with observations on natural omphacites by Smyth et al. (1991), although the infrared spectra of natural omphacites are quite different from the synthetic pure jadeites (Skogby 2006 and references therein). Water solubility reaches a maximum of about 450 ppm by weight at 20 kbar and slowly decreases with increasing pressure to about 100 ppm at 100 kbar. A fit of the experimental data to an equation similar to Equation (11) suggest that water solubility increases with the square root of water fugacity, consistent with the incorporation of hydrogen as isolated OH groups (Table 2).

The most important result of the study by Bromiley and Keppler (2004) is probably that chemical composition has a major effect on water solubility in clinopyroxene. In particular, water solubility is strongly enhanced by the presence of some Ca-Eskola component $Ca_{0.5}\square_{0.5}AlSi_2O_6$. However, a systematic study of water solubility in omphacite throughout the compositional space of natural samples is still lacking. Considering the likely importance of omphacite for recycling water back into the mantle, this may be the most important unsolved problem in calibrating the water solubility in the nominally anhydrous minerals of the upper mantle.

Bromiley et al. (2004) carried out some hydrous annealing experiments of a natural chromian diopside at 1000-1100 °C and 5 to 40 kbar. Water solubility was found to increase with pressure to 229 ppm at 40 kbar, but there is evidence that the solubility law derived from this study (Table 2) reflects some metastable equilibrium dictated by the defect populations inherited in the starting material. An interesting observation of the study by Bromiley et al. was, however, that the ratio of the two bands at 3646 cm^{-1} and at 3434 cm^{-1} is independent of water fugacity, but dependent on oxygen fugacity (Fig. 10). Since water loss from a xenolith during ascent usually involves oxidation of Fe^{2+} to Fe^{3+}, the ratio of these bands therefore could potentially indicate whether a mantle clinopyroxene still preserves its original water content or not.

Water partitioning among upper mantle minerals

Olivine and orthopyroxene are the two main constituents of the upper mantle. The partition coefficient of water between these two phases at water saturation is simply the ratio of the water solubilities in the two phases. Figure 11 shows the calculated partition coefficient for water between olivine and aluminum-saturated orthopyroxene as a function of pressure and temperature. These partition coefficients are based on the solubility law of Kohlstedt et al. (1996) for olivine without any correction for the effect of temperature and on the solubility

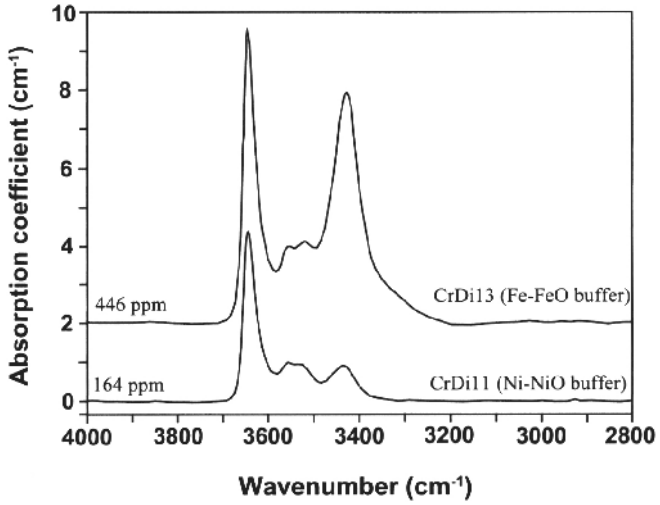

Figure 10. Averaged polarized infrared spectra of chromian diopside annealed in water at 15 kbar and 1100°C under different oxygen fugacities, corresponding to the Ni-NiO and the Fe-FeO-buffer. Clearly, the band at 3434 cm^{-1} is very much enhanced under reducing conditions. The relative intensity of this band can therefore be used as a measure of the oxygen fugacity recorded by the sample. Since the loss of water upon ascent of a xenolith involves oxidation of Fe^{2+} to Fe^{3+}, the relative intensities of the infrared bands could also be used as an indicator of water loss from a mantle clinopyroxene. From Bromiley et al. (2004).

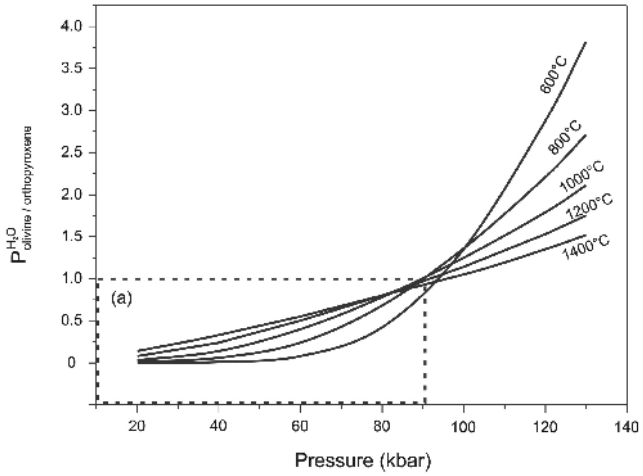

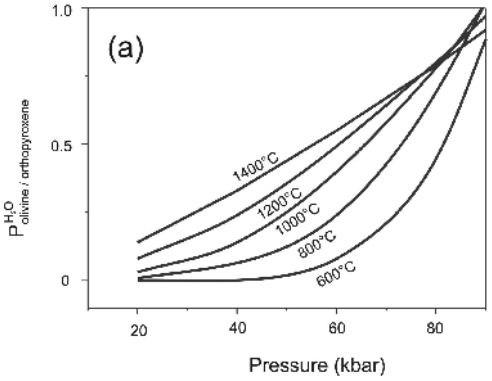

Figure 11. Calculated partition coefficients of water between aluminous orthopyroxene and olivine in equilibrium with an aluminous phase (spinel or garnet, depending on pressure) and under the conditions of water saturation. The calculation is based on the model for water solubility in aluminous orthopyroxene of Mierdel (2006; see Fig. 4) and on the water solubility in olivine as measured by Kohlstedt et al. (1996). After Mierdel (2006).

law of Mierdel (2006) and Mierdel et al. (in prep.) for aluminum-saturated orthopyroxene, which explicitly includes the effect of temperature (see Table 2 for parameters). While water partitions slightly more into olivine at pressures above 90 kbar, it strongly partitions into the aluminous orthopyroxene at lower pressures. Partition coefficients along a typical oceanic and continental geotherm are shown in Figure 12. In the uppermost mantle, water partitions very strongly into the aluminous pyroxenes, particularly along the relatively cold continental geotherm. This effect will be even enhanced if the mantle is far below water saturation, as one would expect. While the solubility of water in olivine is proportional to water fugacity, the part of the solubility of water in pyroxenes which is coupled to Al only increases with the square root of water fugacity. Therefore, at a water activity of 0.1, water solubility in olivine would be reduced by a factor of 10, while water solubility in aluminous orthopyroxene would only be reduced by a factor of about 3. Therefore, water would partition into the aluminous orthopyroxene even three times stronger than at water saturation. In the light of these data, it should not be surprising that pyroxenes from mantle xenoliths often contain much more water than the coexisting olivines.

The calculated partition coefficients in Figure 11 agree quite well with the measured olivine/orthopyroxene partition coefficient of 0.11 ± 0.01 (4 measurements) by Aubaud et al. (2004), measured at 10-20 kbar and 1230-1380 °C.

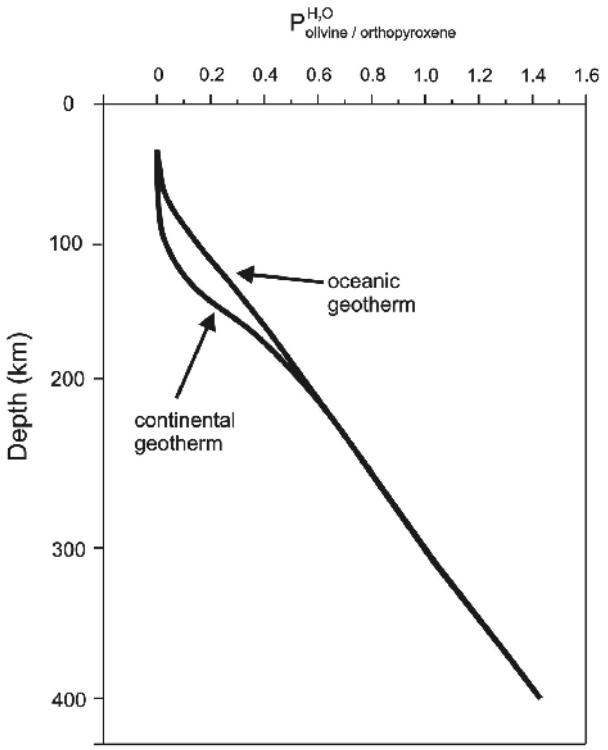

Figure 12. Calculated partition coefficient of water between olivine and aluminous orthopyroxene in equilibrium with spinel or garnet under conditions of water saturation. Shown is the partition coefficient as a function of depth for a continental and an oceanic geotherm. After Mierdel (2006).

If olivine/orthopyroxene partition coefficients were calculated based on the calibration of water solubility in olivine by Mosenfelder et al. (2006), they would increase about three times. This would not, however, change the fact that in the uppermost mantle, most of the water partitions into the aluminous orthopyroxene.

Water storage capacity of the upper mantle and the origin of the Earth´s asthenosphere

Figure 13 shows the water solubility in a model mantle consisting of 60% olivine and 40% aluminum-saturated orthopyroxene as a function of depth for a continental geotherm (Mierdel 2006; Mierdel et al. in prep.). Water solubility in mantle minerals has a pronounced minimum at a depth interval, which coincides with the location of the seismic low-velocity zone. The minimum is due to the sharp decrease of water solubility in aluminum-saturated orthopyroxene with depth, while the water solubility in olivine continuously increases. Figure 13 suggests that in the seismic low-velocity zone, about 1000 ppm of water would be required for a free aqueous fluid to coexist with water-saturated mantle minerals. However, since the temperatures at these depths are already above the water-saturated solidus, the presence of excess water will trigger the formation of a hydrous melt. In this melt, water activity will be significantly reduced, probably to values between 0.1 to 0.3 (Mierdel et al. in prep.). At these reduced water activities, however, the solubility of water in olivine and pyroxene will also be reduced. Therefore, Figure 13 suggests that in depth interval of the seismic low-velocity zone, a few hundred ppm of water are probably sufficient to trigger the formation of a hydrous melt. Partial melting in the low-velocity zone is therefore not related to volatile enrichment, but to a minimum in the solubility of water in mantle minerals. As the water solubility in minerals below and above the low-velocity zone increases, water increasingly partitions into the solid minerals and the melt solidifies. The sharp increase in water solubility above the low-velocity

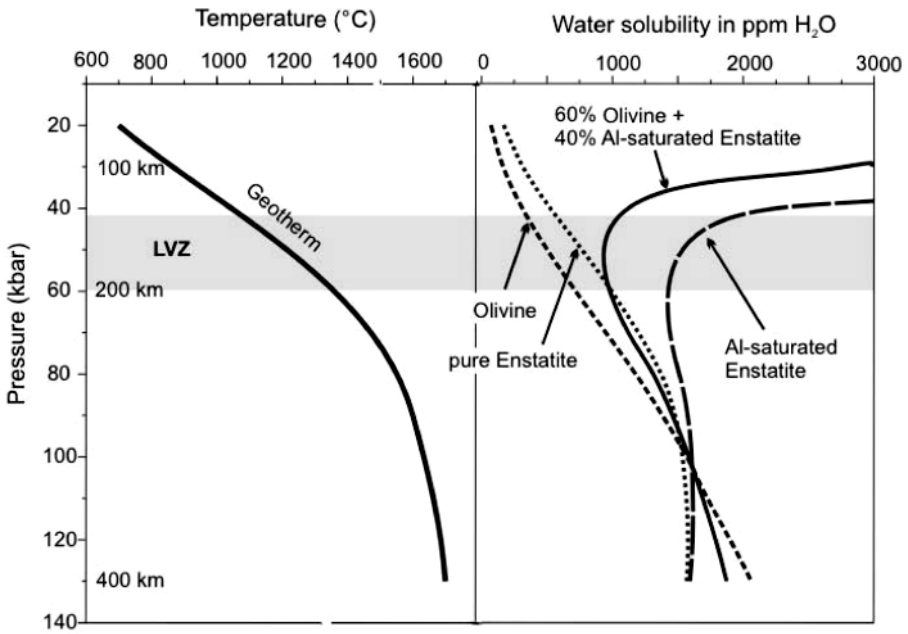

Figure 13. Water solubility along a continental geotherm in a model mantle consisting of a 60:40 mixture of olivine and Al-saturated enstatite. The depth interval of the seismic low velocity zone below continents is shaded. The low velocity zone corresponds to a minimum in water solubility in minerals, suggesting that the excess water forms a partial melt. Water solubility in olivine is after Kohlstedt et al. (1996), water solubility in aluminous enstatite after Mierdel (2006). Diagram after Mierdel (2006) and Mierdel et al. (in prep.).

zone therefore explains why this upper boundary is usually well resolved in seismic data, while on the other hand the gradual increase in water solubility below the low-velocity zone corresponds to the diffuse nature of this seismic boundary. For a hotter, oceanic geotherm, the upper boundary of the low-velocity zone is lifted upwards because of the decrease of water solubility in aluminous orthopyroxene with temperature, again consistent with seismic observations (Mierdel et al. in prep.).

The seismic low-velocity zone is often identified with the asthenosphere, the ductile layer below the lithosphere, which allows the sliding of lithospheric plates required by plate tectonics. The model outlined here suggests that plate tectonics can only exist in a planet with a water-bearing mantle, because without water, no asthenosphere would exist.

Water recycling by subducted slabs

Water recycling into the mantle was already discussed by Ito et al. (1983). Rüpke et al. (2004) recently estimated that most of the water presently residing inside the mantle was actually recycled by subduction. Moreover, they estimated that the global sea level dropped by several hundred meters due to subduction of water since the Cambrian. However, all of these estimates are based on the assumption of widespread serpentinization of the suboceanic mantle. Whether such a serpentinization does indeed occur is uncertain. It may very well be that serpentinization of the suboceanic mantle is only a local phenomenon and therefore, serpentine is not a significant carrier for recycling of water into the mantle. Moreover, even if serpentine is present initially, it will decompose unless the temperature inside the subducted slab remains quite low as during fast subduction of old slabs.

The potential importance of nominally anhydrous minerals in transporting water back into the mantle was probably first pointed out by Lu and Keppler (1997). Even if all hydrous minerals become unstable in the subducted slab at relatively shallow depth, not all water will be lost because the nominally anhydrous minerals will absorb at least part of the water released. According to Lu and Keppler (1997), the amount of water recycled by subducted oceanic crust can be estimated by multiplying the total length of subduction zones on Earth (presently 42 000 km) with the average speed of subduction (presently 5 cm/year) the thickness of the oceanic crust (about 6 km) with the density of the oceanic crust (about 3 g/cm^3) and its water content. For a water content of 1000 ppm, this yields the subduction of 3.78×10^{16} tons or 2.7% of the total ocean mass (1.4×10^{18} tons) over one billion years. If this loss of water were not balanced by outgasing, it would translate into a reduction of global sea level by 100 meters.

The basaltic layer of the subducted oceanic crust consists of eclogite, with pyrope-rich garnet and omphacite being the main constituent minerals. While garnet is unlikely to carry major amounts of water, natural omphacite samples are among the most water-rich nominally anhydrous minerals. A water content of 1000 ppm by weight in the subducted slab would be consistent with observed water contents in natural omphacites of several thousand ppm (Skogby 2006). The precise amount of water subducted in the oceanic crust will depend on the trajectory of the subducted slab in a pressure temperature diagram, which determines the depth of decomposition of hydrous minerals. The water solubility in nominally anhydrous minerals, particularly omphacite, will then determine how much water can be carried down into the mantle. Unfortunately, as noted above, the water solubility in omphacite as a function of pressure, temperature and bulk composition is not yet appropriately calibrated. It is likely, however, that water recycling will vary significantly with the trajectory of the subducted slabs in pressure temperature space, which in turn depends on such parameters such as the age of the slab. It is therefore conceivable that these parameters ultimately contribute to slow variations in the volume of the hydrosphere.

In the considerations above, it was assumed that only the oceanic crust itself would contribute to water recycling into the mantle. However, advective flow of the mantle inside the mantle wedge above the subducted slab may contribute significantly to water recycling, as water released by the subducted slab will hydrate orthopyroxene and olivine in the mantle immediately above the slab. As shown in Figure 13, the water solubility in a bulk mantle consisting of 60% olivine and 40% orthopyroxene will never be much below 1000 ppm. If one assumes that for example, a 60 km thick layer of mantle above the subducted slab were dragged down together with the slab, the amount of water subducted may increase by one order of magnitude as compared to the value calculated above.

Clearly, any kind of accurate estimate of water recycling over geologic time needs to integrate mantle convection models, thermal models of subduction zones, thermodynamic models of the stability of hydrous phases with models of water solubility in minerals such as omphacite. The development of such an integrated model of the Earth's internal water cycle is certainly a major challenge for the coming decade.

WATER IN TRANSITION ZONE MINERALS

Water solubility in wadsleyite and water partitioning between wadsleyite and olivine

Wadsleyite has an unusual structure with a Si_2O_7 group and an oxygen atom that is not attached to a silicate tetrahedon. Smyth (1987) first suggested that this O1 oxygen atom is strongly underbonded and may therefore be a suitable site for protonation. Full protonation of this oxygen atom, charge compensated by magnesium vacancies, would lead to a water content of 3.3 wt% and would therefore make wadsleyite a major storage site for water in the Earth's interior.

Infrared spectroscopic evidence for water in synthetic wadsleyite was first detected by McMillan et al. (1991; about 0.06 wt%) and by Young et al. (1993; 0.06-0.39 wt%). The samples in these early studies, however, were probably not water-saturated. Much higher water contents were later reported by Inoue et al. (1995; 3.1 wt% measured by SIMS), by Kohlstedt et al (1996; up to 2.4 wt% measured by FTIR) and by others. Jacobsen et al. (2005) reported the first polarized FTIR spectra of hydrous wadsleyite (Fig. 14). They appear to be completely consistent with a protonation of the O1 site only, as originally proposed by Smyth (1987), while Kohn et al. (2002) had suggested some disordering of protons over different oxygen atoms. In virtually all studies of hydrous wadsleyite, high water contents were found to correlate with reduced Mg/Si ratios, implying charge balancing of two protons by an Mg^{2+}-vacancy.

Under the pressure and temperature conditions of the transition zone, the meaning of the term water solubility has to be carefully considered. Under these conditions, hydrous fluids and silicate melts are likely to be completely miscible and at realistic transition zone temperatures, solid silicates will never coexist with a water-rich fluid, but with a hydrous silicate melt. Therefore, water solubility can only be defined as the equilibrium water content of a mineral coexisting with a hydrous melt in a phase assemblage that buffers the compositions of all coexisting phases in such a way that the composition of each phase only depends on pressure and temperature. Demouchy et al. (2005) reported the water contents in wadsleyite coexisting with hydrous melt and clinoenstatite in the system MgO-SiO_2-H_2O at 130-180 kbar and 900-1400 °C. In this system, the composition of all phases is buffered, i.e., increasing the amount of water in the charge would only increase the melt fraction, without changing the composition or water content of any of the phases. Therefore, the experimental results from this study can be considered to represent true water solubilities. Figure 15 shows the dependence of water solubility in wadsleyite on temperature. Clearly, water solubility is nearly constant between 900 and 1100 °C, but then drops drastically at higher temperatures. This effect is entirely due to the decrease of water activity in the melt with increasing temperature, because the partition

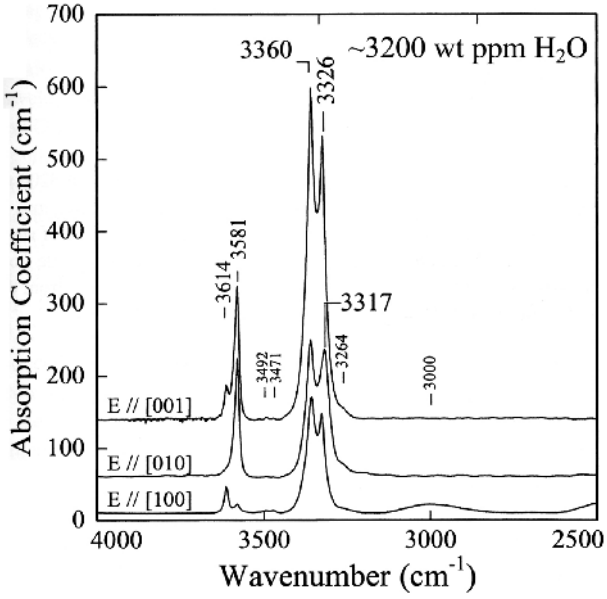

Figure 14. Polarized infrared spectrum of hydrous wadsleyite with 3200 ppm water. From Jacobsen et al. (2005).

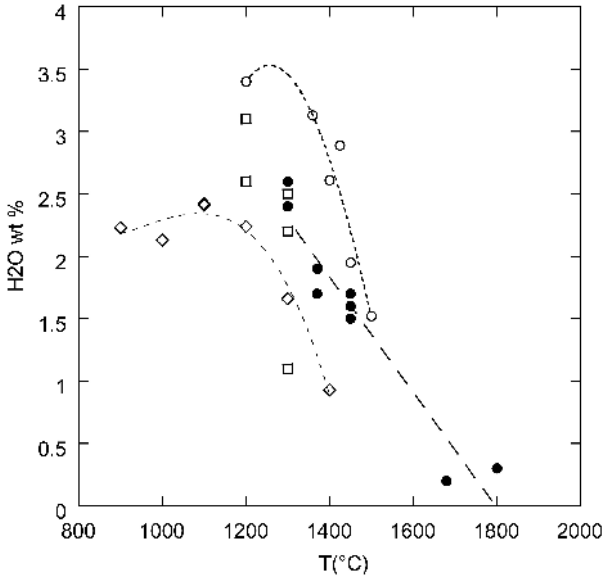

Figure 15. SIMS derived water contents as a function of temperature for pure Mg_2SiO_4 wadsleyite (Inoue et al. 1995: open squares; Demouchy et al. 2005: open diamonds); $(Mg,Fe)_2SiO_4$ wadsleyite in the KLB-1 system (Kawamoto et al. 1996: open circles); and pure Mg_2SiO_4 ringwoodite (Ohtani et al. 2000: filled circles). The decrease in water solubility above 1200 °C is due to a reduced water activity in the melt. Curves are a guide for the eye only.

coefficient of water between wadsleyite and melt remains nearly unchanged ($D_{water}^{wadsleyite/melt}$ = 0.08). On the other hand, pressure was found to have a negligible effect on water solubility in wadsleyite. A similar effect of temperature on water solubility in wadsleyite was observed by Bolfan-Casanova (2005) and Hirschmann et al. (2005) based on a compilation of published analyses from various previous studies (Gasparik 1993; Inoue et al. 1995; Kawamoto et al. 1996; Kohlstedt et al. 1996; Smyth and Kawamoto 1997; Smyth et al. 1997; Chen et al. 2002; Kohn et al. 2002; Litasov and Ohtani 2003; Jacobsen et al. 2005; Demouchy et al. 2005; see Fig. 15). Bolfan-Casanova (2005) and Hirschmann et al. (2005) also noted that water solubility in iron-bearing $(Mg,Fe)_2SiO_4$ wadsleyite may be somewhat higher than in pure Mg_2SiO_4 wadsleyite.

The value of the partition coefficient of water between wadsleyite and olivine primarily depends on the choice of the infrared extinction coefficient used to quantify water contents in olivine. As noted above, the experimental results on water solubility in olivine by Kohlstedt et al. (1996) and by Mosenfelder et al. (2006) are in many aspects comparable, but they yield water contents differing by a factor of about 3, because the former study used extinction coefficients by Paterson (1982) while the latter used the recently determined extinction coefficients by Bell et al. (2003). Water solubility in wadsleyite, on the other hand, is much higher and therefore, it has been quantified by several methods such as SIMS that are independent of infrared measurements. At 120 kbar and 1100 °C, Kohlstedt et al. (1996) report 1510 ppm of water in olivine, while Mosenfelder et al. (2006) find 6399 ppm using the new infrared extinction coefficients. This compares to 2.4 wt% of water in pure Mg_2SiO_4 wadsleyite measured by Demouchy et al. (2005) at 150 kbar and 1100 °C. Since water solubility in wadsleyite appears to be rather insensitive to pressure, these numbers give at 1100 °C $D_{water}^{wadsleyite/olivine}$ of 16 and 3.8, respectively. Since both in wadsleyite and in olivine, proton pairs substitute for Mg^{2+}, water solubility in both phases should be directly proportional to water fugacity. Accordingly,

this partition coefficient should remain constant even if the water activity is reduced at higher temperatures due to a reduced water content of the residual melt. However, the partition coefficient may be further reduced if the water solubility in olivine intrinsically increases with temperature even at constant water fugacity, as suggested by Zhao et al (2004) and Smyth et al (Smyth, pers. comm.), while the intrinsic water solubility in wadsleyite is independent of temperature (Demouchy et al. 2005). Direct SIMS measurements of water contents in coexisting olivine and wasleyite by Chen et al (2002) yielded $D_{water}^{wadsleyite/olivine} = 5$.

The preferential partitioning of water into wadsleyite implies that with increasing water fugacity, the stability field of wadsleyite should grow at the expense of the stability field of olivine, consistent with experimental observations (Chen et al. 2002; Smyth and Frost 2002). The 410 km discontinuity between the upper mantle and the transition zone should therefore be lifted upwards in regions of high water content. In addition, water may broaden the width of the seismic discontinuity (Wood 1995; Smyth and Frost 2002).

Bercovici and Karato (2003) proposed an intriguing model of the chemical evolution of the Earth's mantle based on the different solubility of water in wadsleyite and olivine. They suggested that material upwelling from the transition zone may contain that much water that it cannot be completely accommodated in upper mantle minerals, particularly olivine. Therefore, a partial melt will form on top of the transition zone. This partial melt may extract most incompatible elements out of the upwelling mantle peridotite and may recycle it back into the transition zone or lower mantle. This model is very attractive, because it could reconcile a chemically stratified mantle with whole-mantle convection. The essential requirement of this model is that the water content present in the upper transition zone cannot be dissolved in olivine and the other upper mantle minerals. In the light of the discussion above, this again ultimately depends on the value of the infrared extinction coefficient of water in olivine. If the calibration by Paterson (1982) is accepted, the resulting water solubilities in olivine (Kohlstedt et al. 1996) are sufficiently low to make the Bercovici-Karato model quite plausible. On the other hand, the infrared extinction coefficient by Bell et al. (2003) yields such high values for the water solubility in olivine in the deepest part of the upper mantle (Mosenfelder et al. 2006) that the Bercovici-Karato model would require implausibly high water contents in the transition zone in order to work.

Partitioning of water between wadsleyite and ringwoodite

Mg_2SiO_4 ringwoodite has the spinel structure. Since ordinary spinels are generally among the most water-poor minerals, it was believed for a long time that the water solubility in ringwoodite should be very low. This changed with the work by Kohlstedt et al. (1996) who observed water contents in $(Mg,Fe)_2SiO_4$ ringwoodite up to 2.6 wt% at 19.5 GPa and 1100 °C. Since then, many studies confirmed that ringwoodite may dissolve more than 2 wt% of water (e.g., Kudoh et al. 2000; Ohtani et al. 2000; Smyth et al. 2003), although the mechanism of water incorporation is not completely understood. Infrared spectra of hydrous ringwoodite with water contents up to about 1 wt% show a rather broad absorption band at about 3100 cm^{-1} (Fig. 16), while at higher water contents, additional bands appear at 3345 cm^{-1} and 3645 cm^{-1} (Kohlstedt et al. 1996). The position of the bands at low frequency would be consistent with the incorporation of protons on edges of the tetrahedral site, while the band at 3645 cm^{-1} would be more consistent with protons located on the edge of an octahedral site. Both mechanisms are possible, because X-ray crystal structure refinements of hydrous ringwoodite show some vacancies on the Mg^{2+} site (Smyth et al. 2003), but there is also evidence for Mg^{2+}-Si^{4+}-disordering (Kudoh et al. 2000), i.e., for some Mg^{2+} entering the tetrahedral site, which may involve local charge compensation by two protons.

As with wadsleyite, the observed water contents in ringwoodite cannot be easily interpreted in terms of "solubility," as the coexisting phase is usually a hydrous silicate

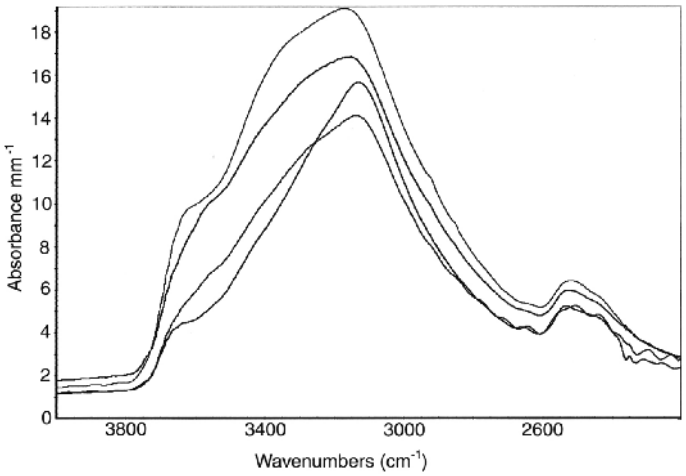

Figure 16. Infrared spectra of hydrous ringwoodite (Fo_{88-90}) with up to 1 wt% water. The spectra shown here are characteristic for ringwoodite with low to moderate water content. At water contents of 2 wt% or above, there is a prominent band at 3645 cm^{-1} which is only present as a shoulder in the spectra shown here. From Smyth et al. (2003).

melt, not an aqueous fluid. Ohtani et al. (2000) observed that the partition coefficient of water between ringwoodite and silicate melt ($D_{water}^{ringwoodite/melt}$) increases from 0.021-0.024 at 1300 °C to 0.04-0.044 at 1450 °C. Together with the data on the partitioning of water between wadsleyite and silicate melt by Demouchy et al. (2005), this would imply that water partitioning between wadsleyite and ringwoodite is strongly temperature dependent, with $D_{water}^{wadsleyite/ringwoodite}$ decreasing from about 4 at 1300 °C to about 2 at 1450 °C and to about 1 at 1600 °C. This would imply that the sharpness of the 520 km discontinuity, if it is related to the wadsleyite-ringwoodite transition, may be a strong function of temperature. Moreover, some repartitioning of water from the lower transition zone to the upper transition zone may have occurred during the cooling of the Earth since the Archean (Demouchy et al. 2005).

Partition coefficients of water between other high-pressure phases

Table 3 shows some partition coefficients of water between various high-pressure phases in the system MgO-SiO_2-H_2O derived from infrared measurements of coexisting phases in high-pressure experiments (after Bolfan-Casanova et al. 2000). Note that while pure SiO_2 stishovite dissolves very little water, water solubility increases very much in the presence of aluminum (Pawley et al. 1993). Also, in stishovite the OH dipole vector is oriented parallel to the *c*-axis, which causes a strong anisotropy of infrared absorption. Water partition coefficients derived from unpolarized infrared measurements are therefore subject to large errors. The infrared spectrum of hydrous majorite shows only one broad band at 3550 cm^{-1}. The infrared spectrum of hydrous akimotoite is shown in Figure 17. A detailed structural model for water incorporation in akimotoite was derived by Bolfan-Casanova et al. (2002a). The 3390 cm^{-1} band is due to an OH group pointing into a tetrahedral void, while the band at 3320 cm^{-1} is due to an OH group located on the triangular face of a vacant octahedron. Bolfan-Casanova (2000) report up to 680 and 445 ppm wt of water in majorite and akimotoite, respectively, which is far below the water content found in wadsleyite and ringwoodite under comparable conditions. Thus the high-pressure polymorphs of $MgSiO_3$ probably do not contribute much to the water storage capacity of the transition zone.

Table 3. Experimentally determined partition coefficients of water among minerals of the lower mantle and the transition zone.

P **(GPa)**	***T*** **(°C)**	**Phase assemblage**	**Partition coefficient**
		----------*System MgO – SiO_2 – H_2O*----------	
15	1300	Wads + Cen + melt	$D^{Wadsleyite/Clinoenstatite} \sim 3.8$
15	1500	Cen + Stish + melt	$D^{Clinoenstatite/Stishovite} \sim 8.2$
17.5	1500	Maj + Stish + melt	$D^{Majorite/Stishovite} \sim 270$
19	1200	Ringw + Stish	$D^{Ringwoodite/Stishovite} \sim 521$
19	1300	Ringw + Akim + Stish + melt	$D^{Ringwoodite/Akimotoite} \sim 21$
21	1500	Akim + Stish + melt	$D^{Akimotoite/Stishovite} \sim 18$
24	1600	Perov + Akim + Stish + melt	$D^{Akimotoite/Perovskite} >> 1$
24	1500	Pe + Perov + melt	$D^{Periclase/Perovskite} > 1$
		----------*System MgO – FeO – SiO_2 – H_2O*----------	
24	1400	Ringw + Perov	$D^{Ringwoodite/Perovskite} \sim 1050$
24	1400	Ringw + Perov + Fe-Pe + melt	$D^{Ringwoodite/Perovskite} \sim 1400$
			$D^{Ferropericlase/Perovskite} \sim 60$

Wads = wadsleyite, Cen = clinoenstatite, Stish = stishovite, Maj = majorite, Ring = ringwoodite, Akim = akimotoite, Perov = $MgSiO_3$ perovskite, Fe-Pe = ferropericlase. After Bolfan-Casanova et al. (2000) and Bolfan-Casanova et al. (2003).

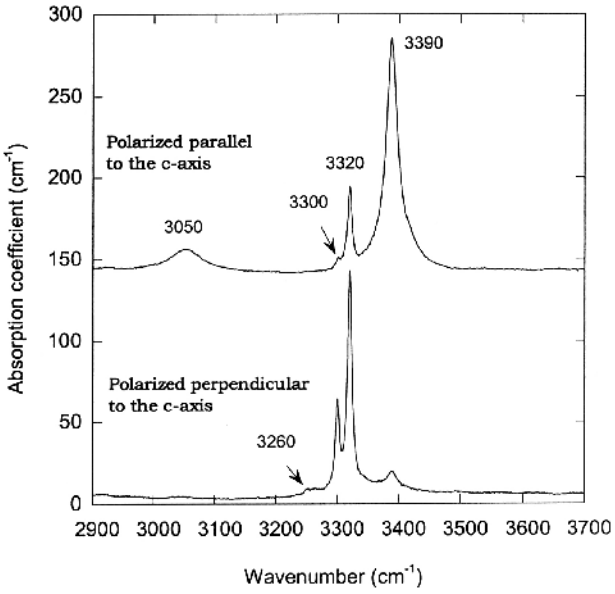

Figure 17. Polarized infrared spectra of $MgSiO_3$ akimotoite containing about 350 ppm of water. From Bolfan-Casanova et al. (2002).

WATER IN MINERALS OF THE LOWER MANTLE

Water in ferropericlase

A peridotitic lower mantle is composed of 80% by volume of orthorhombic magnesium silicate perovskite $(Mg,Fe)(Si,Al)O_3$, 15% of (Mg,Fe)O and 5% of cubic calcium silicate perovskite $CaSiO_3$ (Wood 2000). Unlike the perovskite phases, ferropericlase is stable over a wide range of pressures and temperatures. Moreover, in a simple system MgO-H_2O, the composition of coexisting periclase and water is a function of pressure and temperature only and therefore, equilibrium water contents measured in periclase represent true water solubilities. Although the addition of iron to the system introduces an additional degree of freedom, the system (Mg,Fe)O – H_2O is still invariant, if pressure, temperature, oxygen fugacity and bulk molar Fe/Mg ratio are fixed.

The solubility of water in $(Mg_{0.93}Fe_{0.07})O$ was studied by Bolfan-Casanova et al. (2002b), as a function of pressure from 1.2 to 25 GPa at 1200°C and at Re-ReO_2 buffer conditions. The hydrous ferropericlase samples showed infrared bands at 3320 and 3480 cm^{-1} (Fig. 18), together with a broad band at 3400 cm^{-1} and one peak at ~3700 cm^{-1}. The intensity of the latter feature increases dramatically in areas containing inclusions and is therefore attributed to brucite precipitated upon quenching of the MgO-rich fluid (see also Gonzalez et al. 1982). Whether the broad band at 3400 cm^{-1} is due to structural OH is uncertain, but since the intensity of this band decreases with increasing pressure and becomes very weak at the conditions where ferropericlase is stable in the mantle, it was not included in the thermodynamic model of water solubility (Table 2). The concentration of OH increases as a function of pressure to 20 ppm H_2O by weight (100 H/10^6*Me*, where *Me* = Mg and Fe) at 25 GPa. On the other hand, the ferric iron content decreases, as indicated by Mössbauer spectra, even if oxidizing conditions

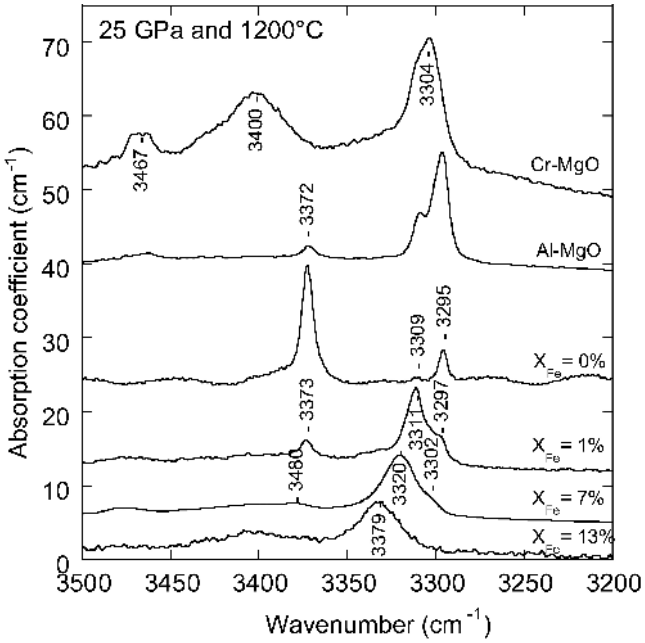

Figure 18. Infrared spectra showing the OH stretching region of periclase with different compositions hydrothermally annealed at 25 GPa and 1200°C. The effect of iron content from X_{Fe} = 0 to 13% p.f.u. is shown as well as the effect of adding trivalent cations to MgO, such as Al^{3+} and Cr^{3+}.

are maintained in the capsule by using the Re-ReO_2 buffer. Thus the Fe^{3+} and OH contents in ferropericlase show opposite trends with pressure. Water solubility increases with the square root of water fugacity (Table 2), indicating the incorporation of water as isolated OH groups. The change in volume of the solid upon hydration is very low (3.95 cm^3/mol).

The effect of iron content on water solubility in ferropericlase was studied by Bolfan-Casanova et al. (2006). They showed that varying the iron content from 1 to 13% has little effect on the solubility of water in ferropericlase at 25 GPa, and the incorporation mechanism appears to be the same, judging from the similarity in the IR spectra (Fig. 18). The main effect of iron is a shift of the infrared absorption bands to higher frequencies. Fe^{3+}/Fe_{tot} decreases with pressure of hydrothermal annealing at 1200 °C for the three compositions studied (X_{Fe} = 0.01, 0.07, 0.13), and the higher the iron content, the higher is the Fe^{3+} content for similar (P, T, f_{O_2}) conditions. To the contrary, increasing temperature from 1200 °C to 1600 °C induces an oxidation of the samples, whereas the OH content decreases. Thus the solubilities of Fe^{3+} and OH are again anticorrelated as a function of increasing temperature.

The infrared spectrum of MgO hydrothermally annealed at 25 GPa and 1200 °C is also shown in Figure 18. The spectrum is mainly composed of three bands at 3372, 3309 and 3296 cm^{-1}. When comparing the OH absorption bands in pure MgO with those of MgO doped with Al^{3+} or Cr^{3+} at 1200 °C, one observes that the band at 3372 cm^{-1} is intrinsic to pure MgO. This band is also present in the spectra of Al-, Cr-, and Fe-doped MgO but with much lower intensity. Again, in Cr-doped MgO, a broad band centered around 3400 cm^{-1} is observed, the origin of which is still not understood. Thus, the effect of doping with trivalent cations is to increase the intensity of the bands at 3309 and 3296 cm^{-1}, showing that one important mechanism of H incorporation in MgO is via coupling with trivalent cations such as Al^{3+} and Cr^{3+}, while in (Mg,Fe)O the concentrations of Fe^{3+} and H^+ are anticorrelated.

At room pressure, under relatively oxidizing conditions, the most stable ionic defect species in anhydrous (Mg,Fe)O are cation vacancies and ferric iron in octahedral coordination (Gourdin and Kingery 1979). Tetrahedrally coordinated ferric iron is stabilized in Fe-rich compositions (Jacobsen et al. 2002). At low iron contents or low ferric iron contents, the point defect concentrations will be dominated by impurities, particularly trivalent cations such as Al^{3+} in octahedral coordination (see Mackwell et al. 2005). In the dry case, the incorporation of such trivalent cations is charged balanced by the creation of magnesium vacancies. H^+ probably enters periclase coupled to trivalent cations in the octahedral site according to the substitution mechanism $2\ Mg^{2+} \leftrightarrow M^{3+} + H^+$, in agreement with the observed exponent ½ in the water fugacity term. The fact that this mechanism is not very efficient for ferric iron might be due to the low fraction of Fe^{3+}/Fe_{tot} in ferropericlase at high pressures.

Water in magnesium silicate perovskite

Evidence for structurally bound H in $MgSiO_3$ perovskite was first reported by Meade et al. (1994) based on IR studies of single crystals quenched from an H_2O-rich melt. Two pleochroic bands at 3483 and 3423 cm^{-1} were observed consistent with 60 ppm H_2O by weight (700 ± 170 H/10^6 Si).

Bolfan-Casanova et al. (2000) did not detect any OH peak in $MgSiO_3$ perovskite in an extensive experimental study performed under various conditions in the MgO-SiO_2-H_2O system, even when the perovskite coexisted with other minerals that clearly contained water. For example, while $MgSiO_3$ akimotoite coexisting with $MgSiO_3$ perovskite in a sample synthesized at 24 GPa and 1600°C, contained up to 425 ppm wt H_2O, the perovskite was essentially dry. Experiments where MgO coexisted with perovskite at 24 GPa and 1500 °C, yield the same result (Table 3). The spectrum of periclase displayed two very sharp bands located at 3295 and 3372 cm^{-1}, corresponding to ~2 ppm wt H_2O. Bolfan-Casanova et al. (2000) argued that the H content observed by Meade et al. (1994) was not in equilibrium

because the sample was allowed to equilibrate only for a few minutes. Litasov et al. (2003) also studied $MgSiO_3$ perovskite at 25 GPa and 1300°C and observed the bands at 3423 and 3482 cm^{-1}, together with a more intense band at 3448 cm^{-1} and a weaker one at 3397 cm^{-1}. They calculated a water content of about 40 ppm wt H_2O.

It is now probably generally agreed that $MgSiO_3$ perovskite in the simple MgO-SiO_2-H_2O system dissolves only very little water, although the available experimental results are difficult to interpret in terms of a thermodynamically well-defined solubility. The somewhat higher water contents observed by Litasov et al.(2003) as compared to Bolfan-Casanova et al. (2000) could reflect a decrease of water solubility with temperature. Alternatively, they could be due to differences water activity or MgO activity. Ross et al. (2003) studied the electron density distribution in a number of high-pressure silicates and suggested that $MgSiO_3$ perovskite has only one potential docking site for hydrogen. The OH vector is in the (110) plane and hydrogen incorporation probably requires a vacant Mg site, implying that water solubility may be reduced under conditions of high MgO activity, i.e., when perovskite coexists with MgO as in some of the experiments by Bolfan-Casanova et al. (2000).

In the system MgO-FeO-SiO_2-H_2O, the IR spectra of $(Mg,Fe)SiO_3$ perovskite synthesized at 24 GPa and 1400°C display only one very weak peak, at 3388 cm^{-1} (Bolfan-Casanova et al. 2003), yielding 2 ppm wt water (Fig. 19). This study also determined the partition coefficient of water between $(Mg,Fe)_2SiO_4$ ringwoodite and $(Mg,Fe)SiO_3$ perovskite to be ~1050.

The effect of aluminum on water solubility in $MgSiO_3$ perovskite is subject of a major debate. It has been suggested that the incorporation of trivalent ions, especially Al^{3+}, will enhance the solubility of hydrogen in magnesium silicate perovskite (Navrotsky 1999). This idea is based on the observation that in ceramic perovskites the trivalent cation occupies the *B* site in the ABO_3 structure, resulting in the creation of oxygen vacancies. These oxygen vacancies may then be filled by OH groups. Ultimately, this would be equivalent to a substitution where Al^{3+} and H^+ replace Si^{4+}. However, the picture may not be that simple in magnesium silicate perovskite as Al^{3+} can also enter the *A* site. Also, the coupling of Al^{3+}

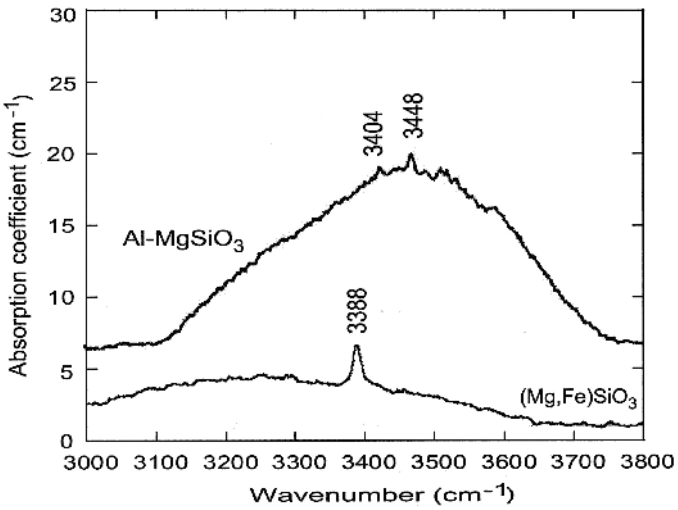

Figure 19. Infrared spectra showing the OH stretching region of perovskite $(Mg_{0.98}Fe_{0.02})SiO_3$ after Bolfan-Casanova et al. (2003) and of $(Mg,Si,Al)O_3$ perovskite containing 4.4 wt% Al_2O_3 after Litasov et al. (2003). Samples were synthesized at 25 GPa and 1400 and 1200 °C, respectively. The origin of the broad band is not fully understood, it may be related to inclusions of a separate phase.

and Fe^{3+} plays an important role in the point defect chemistry of perovskite (Lauterbach et al. 2000). Litasov et al. (2003) find that in (Al,Fe)-perovskite, coupling of Al^{3+} with Fe^{3+} (up to 60% of the total iron being ferric) controls the amount of oxygen vacancies. In perovskite grown from a starting material of MORB composition, the Fe contents are high enough to charge compensate the Al^{3+} defects on the *B* site by Fe^{3+} defects on the A site.

Litasov et al. (2003) analysed Al-perovskites containing 2, 4.5 and 7.2 wt% Al_2O_3, synthesized at temperatures of 1200-1400 °C and pressures of 25-26 GPa. They report OH peaks located at 3397, 3404 and 3448 cm^{-1}, superimposed on a very broad band centered around 3400-3450 cm^{-1}, the intensity of which increases with Al_2O_3 content in the perovskite (Fig. 19). The integrated water contents are 100, 1100 and 1400 ppm H_2O by weight in the order of increasing aluminum content. However, it seems that the intensity of the sharp peaks decreases with aluminum. If only these peaks are considered as structural water in perovskite, the water contents in Al-perovskite would accordingly decrease with Al.

Litasov et al. (2003) also studied Al-Fe bearing perovskites in the MORB and peridotite systems. In the MORB system, perovskites synthesized at pressures of 25-26 GPa and temperatures of 1000, 1200 and 1300 °C display IR peaks at 3397, 3423 and 3448 cm^{-1}. The water content associated with the most intense band, at 3397 cm^{-1}, is 40-110 ppm wt H_2O, decreasing with increasing temperature of synthesis. In perovskites synthesized at 25 GPa and temperatures of 1400 and 1600°C in the peridotite system, the IR bands are more intense than in MORB related perovskite and yield 1400-1800 ppm wt H_2O, with water contents decreasing slightly with increasing temperature. These perovskites generally display very broad bands in the IR spectra. Murakami et al. (2002) reported about 0.2 wt% water in $MgSiO_3$ perovskite and up to 0.4 wt% water in amorphized $CaSiO_3$ perovskite grown in a natural peridotitic composition at ~25 GPa and 1600-1650°C. The IR absorption features are very broad with a major broad band centered on 3400 cm^{-1} and a sharp peak at 3690 cm^{-1}. The latter band resembles the band of brucite $Mg(OH)_2$ at 3698 cm^{-1} (brucite microinclusions have also been identified in (Mg,Fe)O hydrothermally annealed at high pressures and temperatures, see above). The infrared spectra measured on different crystals display different intensities, and the SIMS measurements also show a large scatter in water contents (from 0.1 to 0.36 wt% H_2O). These heterogeneities either mean that the samples are not homogeneous in water content, which means that they are not in equilibrium, or that the signal arises from an impurity phases.

Whether aluminous perovskite is indeed able to dissolve much more water than pure $MgSiO_3$ perovskite entirely depends on the interpretation of the IR spectra. The high water contents reported for experimental samples are always due to very broad infrared bands. Although it is possible that such broad bands may be caused by OH point defects, a number of observations suggest that these bands may be due to inclusions of a second phase: (1) Murakami et al. (2002) found this band both in coexisting ferropericlase and in perovskite and observed a significant pleochroism in both phases, despite the fact that ferropericlase is cubic. (2) Bolfan-Casanova et al. (2003) demonstrated that the broad bands are strong only in those parts of perovskite crystals that appear milky under the microscope, while they are not found in the infrared spectra taken on perfectly clear spots. (3) The same authors also demonstrated that some of the milky parts of synthetic aluminous perovskite show Raman peaks of superhydrous phase B and that the infrared peaks of this phase coincide with the major OH peaks reported for aluminous perovskite. Based on these observations, we tentatively conclude that water solubility in aluminous perovskite is generally very low and the high water contents reported in the literature are probably due to impurities.

The distribution of water at the 660 km discontinuity

Based on the discussion above, it appears that both ferropericlase and particularly magnesium silicate perovskite dissolve much less water than ringwoodite under comparable conditions. No experimental data are available on water in calcium silicate perovskite.

However, Ross et al. (2003) could not locate any suitable docking site for hydrogen in the structure of calcium silicate perovskite based on its electron density distribution. This would suggest that this phase is not a significant storage site for water in the mantle. The data on water solubility in ferropericlase together with the data on water partitioning between ringwoodite and perovskite and between perovskite and ferropericlase (Table 3) suggest a bulk partition coefficient between ringwoodite and perovskite + ferropericlase $D_{water}^{ringwoodite/(ferropericlase+perovskite)}$ of about 710. This implies that the 660 km discontinuity should be broadened and shifted to greater depth in the presence of water. Compared to the transition zone, the bulk storage capacity of the lower mantle is probably negligible.

THE EQUILIBRIUM DISTRIBUTION OF WATER IN THE EARTH'S INTERIOR

Measurements of water solubility in minerals cannot directly yield the actual water content of the mantle. They only constrain the maximum water storage capacity of the mantle and the partitioning of water between various phases. However, if one assumes chemical equilibrium throughout the mantle, partitioning data can be used to calculate the water distribution in the mantle based on independent estimates of the actual water content in one of the major mantle reservoirs. Whether the water distribution in the mantle is indeed close to equilibrium, is uncertain, although the relatively high diffusion coefficients of hydrogen in minerals (Ingrin and Blanchard 2006, this volume) and the high mobility of aqueous fluids could help to establish equilibrium over geologic timescales. Richard et al. (2002) have investigated the distribution of water in the Earth's interior using convection models together with data on the diffusion of water in minerals. From their calculations, it appears that an equilibrium distribution of water in the mantle is only possible if aqueous fluids, hydrous silicate melts or hydrous carbonatite melts are involved in the transport of water.

One model of equilibrium water distribution in the mantle is given in Table 4, after Bolfan-Casanova (2000). Key input parameters in this model are a bulk water content of 250 ppm in the upper mantle (consistent with estimates from both mantle xenoliths and analyses of MORB glasses), a partition coefficient of water between wadsleyite and olivine of 20 and a very low water solubility in lower mantle phases. The predicted water concentration in the transition zone of 1400 ppm is consistent with recent estimates based on electrical conductivity (Huang et al. 2005; see also Hirschmann 2006).

On the other hand, one may assume a water content of 1500 ppm in wadsleyite of the upper transition zone from electrical conductivity measurements (Huang et al. 2005) as a starting point for the calculation. Together with a water partition coefficient of 3.8 between wadsleyite and olivine, which may result from the new calibration of infrared extinction coefficients in olivine according to Bell et al. (2003), this yields a water content in upper mantle olivine of 395 ppm. While this appears significantly higher than most estimates for water in the MORB

Table 4. A model for the equilibrium distribution of water in the mantle.

Reservoir	Mass fraction of the Earth	Water content (ppm by weight)	Mass of water (10^{20} kg H_2O)	% of ocean mass
Upper mantle	0.103	~ 250	1.54	11
Transition zone	0.075	~ 1400	6.27	45
Lower mantle	0.492	~ 10	0.29	2

From Bolfan-Casanova (2000); mass of the Earth = 5.97×10^{23} kg, mass of the oceans = 1.4×10^{21} kg

source, it is within the range of water contents inferred for some enriched mantle sources (up to 700 ppm, see review by Bolfan-Casanova 2005 and references therein).

ACKNOWLEDGMENTS

Much of the work presented here has been supported by German Science Foundation (DFG; Gerhard Hess Award and Leibniz Award to HK) and by the EU Hydrospec Network organized by Jannick Ingrin. A review by Marc Hirschmann helped to improve the manuscript.

REFERENCES

Ackermann L, Cemic L, Langer K (1983) Hydrogarnet substitution in pyrope: a possible location for "water" in the mantle. Earth Planet Sci Lett 62:208-214

Aubaud C, Hauri EH, Hirschmann MM (2004) Hydrogen partition coefficients between nominally anhydrous minerals and basaltic melts. Geophys Res Lett 31:L20611, doi:10.1029/2004GL021341

Bai Q, Kohlstedt DL (1992) Substantial hydrogen solubility in olivine and implications for water storage in the mantle. Nature 357:672-674

Bai Q, Kohlstedt DL (1993) Effects of chemical environment on the solubility and incorporation mechanism for hydrogen in olivine. Phys Chem Minerals 19:460-471

Bell DR, Rossman GR (1992) Water in Earth's mantle: The role of nominally anhydrous minerals. Science 255: 1391-1397

Bell DR, Rossman GR, Maldener J, Endisch D, Rauch F (2003) Hydroxide in olivine: A quantitative determination of the absolute amount and calibration of the IR spectrum. J Geophys Res 108 (B2):2105, doi:10.1029/2001JB000679

Bercovici D, Karato S-I (2003) Whole-mantle convection and the transition-zone water filter. Nature 425:39-44

Berry AJ, Herrmann J, O'Neill H St C, Foran GJ (2005) Fingerprinting the water site in mantle olivine. Geology 33:869-872

Bolfan-Casanova N (2000) The distribution of water in the Earth's mantle: An experimental and infrared spectroscopic study. Ph. D. thesis, University of Bayreuth.

Bolfan-Casanova N (2005) Water in the Earth's mantle. Mineral Mag 69:229-257

Bolfan-Casanova N, Keppler H, Rubie DC (2000) Water partitioning between nominally anhydrous minerals in the MgO-SiO_2-H_2O system up to 24 GPa: Implications for the distribution of water in the Earth´s mantle. Earth Planet Sci Lett 182:209-221

Bolfan-Casanova N, Keppler H, Rubie DC (2002a) Hydroxyl in $MgSiO_3$ akimotoite: A polarized and high-pressure IR study. Am Mineral 87:603-608

Bolfan-Casanova N, Mackwell S, Keppler H, McCammon CA, Rubie DC (2002b) Pressure dependence of H solubility in magnesiowustite up to 25 GPa: Implications for the storage of water in the Earth's lower mantle. Geophys Res Lett 29:1029-1032

Bolfan-Casanova N, Keppler H, Rubie DC (2003) Water partitioning at the 660 km discontinuity and evidence for very low water solubility in magnesium silicate perovskite. Geophys Res Lett 30(17):1905

Bolfan-Casanova N, McCammon C, Mackwell S (in press) Water in transition zone and lower mantle minerals *In*: The Earth's deep water cycle. Jacobsen S, Marone F (eds) American Geophysical Union Monograph, in press

Bromiley GD, Keppler H (2004) An experimental investigation of hydroxyl solubility in jadeite and Na-rich clinopyroxenes. Contrib Mineral Petrol 147:189-200

Bromiley GD, Keppler H, McCammon C, Bromiley FA, Jacobsen SD (2004) Hydrogen solubility and speciation in natural, gem-quality chromian diopside. Am Mineral 89:941-949

Bureau H, Keppler H (1999) Complete miscibility between silicate melts and hydrous fluids in the upper mantle: experimental evidence and geochemical implications. Earth Planet Sci Lett 165:187-196.

Chen J, Inoue T, Yurimoto H, Weidner DJ (2002) Effect of water on olivine-wadsleyite phase boundary in the $(Mg,Fe)_2SiO_4$ system. Geophys Res Lett 29:1875, doi:10.1029/2001GL014429

Dankwerth PA, Newton RC (1978) Experimental determination of the spinel to garnet peridotite reaction in the system MgO-Al_2O_3-SiO_2 in the range 900 °C-1100 °C and Al_2O_3 isopleths of enstatite in the spinel field. Contrib Mineral Petrol 66:189-201

Demouchy S, Deloule E, Frost DJ, Keppler H (2005) Pressure and temperature dependence of water solubility in Fe-free wadsleyite. Am Mineral 90:1084-1091

Freda C, Baker DR, Ottolini L (2001) Reduction of water loss from gold-palladium capsules during piston-cylinder experiments by use of pyrophyllite powder. Am Mineral 86:234-237
Gasparik T (1993) The role of volatiles in the transition zone. J Geophys Res 98:4287-4299
Gasparik T (2003) Phase Diagrams for Geoscientists: An Atlas of the Earth Interior. Springer
Gonzalez R, Chen Y, Tsang KL (1982) Diffusion of deuterium and hydrogen in doped and undoped MgO crystals Phys Rev B 26:4637-4645
Gourdin WH, Kingery WD (1979) The defect structure of MgO containing trivalent defect: solutes shell model calculations. J Material Sci 14:2053-2073
Hirschmann MM (2006) A wet mantle conductor? Nature 439:E3, doi:10.1038/nature04528
Hirschmann MM, Aubaud C, Withers AC (2005) Storage capacity of H_2O in nominally anhydrous minerals in the upper mantle. Earth Planet Sci Lett 236:167-181
Huang XG, Xu YS, Karato SI (2005) Water content in the transition zone from electrical conductivity of wadsleyite and ringwoodite. Nature 434:746-749
Ingrin J, Blanchard M (2006) Diffusion of hydrogen in minerals. Rev Mineral Geochem 62:291-320
Ingrin J, Skogby H (2000) Hydrogen in nominally anhydrous upper-mantle minerals: concentration levels and implications. Eur J Mineral 12:543-570
Inoue T, Yurimoto H, Kudoh Y (1995) Hydrous modified spinel $Mg_{1.75}SiH_{0.5}O_4$ – A new water reservoir in the mantle transition region. Geophys Res Lett 22:117-120
Ito E, Harris DM, Anderson AT (1983) Alteration of oceanic crust and geologic cycling of chlorine and water. Geochim Cosmochim Acta 47:1613-1624
Jacobsen SD, Reichmann HJ, Spetzler HA, Mackwell SJ, Smyth JR, Angel RJ, McCammon CA (2002) Structure and elasticity of single-crystal (Mg,Fe)O and a new method of generating shear waves for gigahertz ultrasonic interferometry. J Geophys Res 107 B: Art. No. 2037
Jacobsen SD, Demouchy S, Frost D, Boffa Ballaran T, Kung J (2005) A systematic study of OH in hydrous wadsleyite from polarized FTIR spectroscopy and single-crystal X-ray diffraction: Oxygen sites for hydrogen storage in Earth's interior. Am Mineral 90:61-70
Johnson EA, Rossman GR (2004) A survey of hydrous species and concentrations in igneous feldspars. Am Mineral. 89:586-600
Kawamoto T, Hervig RL, Holloway JR (1996) Experimental evidence for a hydrous transition zone in the early Earth's mantle. Earth Planet Sci Lett 142:587-592
Kessel R, Schmidt MW, Ulmer P, Pettke T (2005) Trace element signature of subduction-zone fluids, melts and supercritical liquids at 120-180 km depth. Nature 437:724-727
Kohlstedt DL, Mackwell SJ (1998) Diffusion of hydrogen and intrinsic point defects in olivine. Z Phys Chem 207:147-162
Kohlstedt DL, Keppler H, Rubie DC (1996) Solubility of water in the α, β, and γ phases of $(Mg,Fe)_2SiO_4$. Contrib Mineral Petrol 123:345-357
Kohn SC, Brooker RA, Frost DJ, Slesinger AE, Wood BJ (2002) Ordering of hydroxyl defects in hydrous wadsleyite (β-Mg_2SiO_4). Am Mineral 87:293-301
Kohn SC, Roome BM, Smith ME, Howes AP (2005) Testing a potential mantle geohygrometer; the effect of water on the intracrystalline partitioning of Al in orthopyroxene. Earth Planet Sci Lett 238:342-350
Kudoh Y, Kuribayashi T, Mizobata H, Ohtani E (2000) Structure and cation disorder of hydrous ringwoodite, γ-$Mg_{1.89}Si_{0.98}H_{0.30}O_4$. Phys Chem Minerals 27:474-479
Lager GA, Marshall WG, Liu Z, Downs RT (2005) Re-examination of the hydrogarnet structure at high pressure using neutron powder diffraction and infrared spectroscopy. Am Mineral 90:639-644
Lauterbach S, McCammon C, van Aken P, Langenhorst F, Seifert F (2000) Mössbauer and ELNES spectroscopy of $(Mg,Fe)(Si,Al)O_3$ perovskite: a highly oxidized component of the lower mantle. Contrib Mineral Petrol 138:17-26
Lemaire C, Kohn SC, Brooker RA (2004) The effect of silica activity on the incorporation mechanism of water in synthetic forsterite: a polarized infrared spectroscopic study. Contrib Mineral Petrol 147:48-57
Litasov K, Ohtani E (2003) Stability of various hydrous phases in CMAS pyrolite-H_2O system up to 25 GPa. Phys Chem Minerals 30:147-156
Litasov K, Ohtani E, Langenhorst F, Yurimoto H, Kubo T, Kondo T (2003) Water solubility in Mg-perovskites and water storage capacity in the lower mantle. Earth Planet Sci Lett 211:189-203
Lu R, Keppler H (1997) Water solubility in pyrope to 100 kbar. Contrib Mineral Petrol 129:35-42
MacGregor ID (1974) The system MgO-Al_2O_3-SiO_2: Solubility of Al_2O_3 in enstatite for spinel and garnet peridotite compositions. Am Mineral 59:110-119
Mackwell S, Bystricky M, Sproni C (2005) Fe-Mg Interdiffusion in (Mg,Fe)O. Phys Chem Mineral 32:418-425
Matsyuk SS, Langer K (2004) Hydroxyl in olivines from mantle xenoliths in kimberlites of the Siberian platform. Contrib Mineral Petrol 147:413-437
Matveev S, O´Neill H St C, Ballhaus C, Taylor WR, Green DH (2001) Effect of silica activity on OH^- IR spectra of olivine: Implications for low-α–SiO_2 mantle metasomatism. J Petrol 42:721-729

Matveev S, Portnyagin M, Ballhaus C, Brooker R, Geiger CA (2005) FTIR spectrum of phenocryst olivine as an indicator of silica saturation in magmas. J Petrol 46:603-614
McMillan PF, Akaogi M, Sato RK, Poe B, Foley J (1991) Hydroxyl groups in β-Mg_2SiO_4. Am Mineral 76: 354-360
Meade C, Reffner JA, Ito E (1994) Synchrotron infrared absorbance measurements of hydrogen in $MgSiO_3$ perovskite. Science 264:1558-1560
Mibe K, Fujii T, Yasuda A (2002) Composition of aqueous fluids coexisting with mantle minerals at high pressure and its bearing on the differentiation of the Earth's upper mantle. Geochim Cosmochim Acta 66: 2273-2285
Mierdel K (2006) Wasserlöslichkeit in Enstatit. PhD thesis, University of Tübingen
Mierdel K, Keppler H (2004) The temperature dependence of water solubility in enstatite. Contrib Mineral Petrol 148:305-311
Miller GH, Rossman GR, Harlow GE (1987) The natural occurrence of hydroxide in olivine. Phys Chem Minerals 14:461-472
Mosenfelder JL, Deligne NI, Asimow PD, Rossman GR (2005) Hydrogen incorporation in olivine from 2-12 GPa. Am Mineral 91:285-294
Murakami M, Hirose K, Yurimoto H, Nakashima S, Takafuji N (2002) Water in the Earth's lower mantle. Science 295:1885-1887
Navrotsky A (1999) A lesson from ceramics. Science 284:1788-1789
Ohtani E, Mizobata H, Yurimoto H (2000) Stability of dense hydrous magnesium silicate phases in the systems Mg_2SiO_4-H_2O and $MgSiO_3$-H_2O at pressure up to 27 GPa. Phys Chem Minerals 27:533-544
Paterson MS (1982) The determination of hydroxyl by infrared absorption in quartz, silicate glasses and similar materials. Bull Minéral 15:20-29
Pawley AR, McMillan PF, Holloway JR (1993) Hydrogen in stishovite, with implications for mantle water content. Science 261:1024-1026
Perkins D, Holland TJB, Newton RC (1981) The Al_2O_3 content of enstatite in equilibrium with garnet in the system MgO-Al_2O_3-SiO_2 at 15-40 kbar and 900-1600 °C. Contrib Mineral Petrol 78:99-109
Rauch M (2000) Der Einbau von Wasser in Pyroxene. PhD thesis, University of Bayreuth
Rauch M, Keppler H (2002) Water solubility in orthopyroxene. Contrib Mineral Petrol 143:525-536
Richard G, Monnereau M, Ingrin J (2002) Is the transition zone an empty water reservoir? Inferences from numerical model of mantle dynamics. Earth Planet Sci Lett 205:37-51
Ross NL, Gibbs GV, Rosso K (2003) Potential docking sites and positions of hydrogen in high-pressure silicates. Am Mineral 88:1452-1459
Rossman GR, Aines RD (1991) The hydrous components in garnets: Grossular-hydrogrossular. Am Mineral 76: 1153-1164
Rüpke LH, Phillips Morgan JP, Hort M, Connolly JAD (2004) Serpentine and the subduction zone water cycle. Earth Planet Sci Letters 223:17-34
Shen A, Keppler H (1997) Direct observation of complete miscibility in the albite-H_2O system. Nature 385: 710-712
Skogby H (2006) Water in natural mantle minerals I: pyroxenes. Rev Mineral Geochem 62:155-167
Smyth JR (1987) β-Mg_2SiO_4: A potential host for water in the mantle? Am Mineral 72:1051-1055
Smyth JR, Frost DJ (2002) The effect of water on the 410-km discontinuity: an experimental study. Geophys Res Lett 29:1485, doi:10.1029/2001GL014418
Smyth JR, Kawamoto T (1997) Wadsleyite II, a new high pressure hydrous phase in the peridotite-H2O system. Earth Planet Sci Lett 146:E9-E16
Smyth J, Bell D, Rossman G (1991) Incorporation of hydroxyl in upper-mantle clinopyroxenes. Nature 351: 732-735
Smyth JR, Kawamoto T, Jacobsen SD, Swope RJ, Hervig RL, Holloway JR (1997) Crystal structure of monoclinic hydrous wadsleyite, β-$(Mg,Fe)_2SiO_4$. Am Mineral 82:270-275
Smyth JR, Holl CM, Frost DJ, Jacobsen SD, Langenhorst F, McCammon CA (2003) Structural systematics of hydrous ringwoodite and water in Earth´s interior. Am Mineral 88:1402-1407
Stalder R (2002) Synthesis of enstatite single crystals at high pressure. Eur J Mineral 14:637-640
Stalder R (2004) Influence of Fe, Cr and Al on hydrogen incorporation in orthopyroxene. Eur J Mineral 16: 703-711
Stalder R, Skogby H (2002) Hydrogen incorporation in enstatite. Eur J Mineral 14:1139-1144
Stalder R, Klemme S, Ludwig T, Skogby H (2005) Hydrogen incorporation in orthopyroxene: interaction of different trivalent cations. Contrib Mineral Petrol 150:473-485
Sykes D, Rossman GR, Veblen DR, Grew ES (1994) Enhanced H and F incorporation in borian olivine. Am Mineral 79:904-908
Truckenbrodt J, Johannes W (1999) H_2O loss during piston-cylinder experiments. Am Mineral 84:1333-1335
Withers AC, Wood BJ, Carroll MR (1998) The OH content of pyrope at high pressure. Chemical Geology 147: 161-171

Wood BJ (1995) The effect of H_2O on the 410-kilometer seismic discontinuity. Science 268:74-76
Wood BJ (2000) Phase transformations and partitioning relations in peridotite under lower mantle conditions. Earth Planet Sci Lett 174:341-354
Yamada A, Inoue T, Irifune T (2004) Melting of enstatite from 13 to 18 GPa under hydrous conditions. Phys Earth Planet Int 147:45-56
Young TE, Green HW, Hofmeister AM, Walker D (1993) Infrared spectroscopic investigation of hydroxyl in β-$(Mg,Fe)_2SiO_4$ and coexisting olivine: Implications for mantle evolution and dynamics. Phys Chem Minerals 19:409-422
Zhao YH, Ginsberg SB, Kohlstedt DL (2004) Solubility of hydrogen in olivine: dependence on temperature and iron content. Contrib Mineral Petrol 147:155-161